

1 **Lagrangian studies of marine production: a multi-method assessment of**
2 **productivity relationships in the California Current Ecosystem upwelling**
3 **region**

4

5 Sven A Kranz^{1,*}, Seaver Wang², Thomas B Kelly¹, Michael R Stukel^{1,3}, Ralf Goericke⁴, Michael
6 R. Landry⁴, Nicolas Cassar²

7

8 ¹Dept. of Earth, Ocean & Atmospheric Sciences, Florida State University, Tallahassee, FL

9 ²Division of Earth and Ocean Sciences, Duke University, Durham, NC

10 ³Center for Ocean-Atmospheric Prediction Studies, Florida State University, Tallahassee, FL

11 ⁴Integrative Oceanography Division, Scripps Institution of Oceanography, La Jolla, CA

12

13 * Corresponding Author: Sven A Kranz (skranz@fsu.edu)

14

15 Keywords: Gross Primary Production, Long Term Ecological Research, Equilibrium Inlet Mass
16 spectrometry, Carbon Export, Net Community Production,

17 Index Terms:

18 **4227 Diel, seasonal, and annual cycles, 0460 Marine systems, 0414 Biogeochemical cycles,**

19 **processes, and modeling, 4806 Carbon cycling, 4820 Gases**

20

21 **Abstract**

22 A multi-method process-oriented investigation of diverse productivity measures in the California
23 Current Ecosystem (CCE) Long-Term Ecological Research study region, a complex physical
24 environment, is presented. Seven multi-day deployments covering a transition region from high
25 to low productivity were conducted over two field expeditions (spring 2016 and summer 2017).
26 Employing a Lagrangian study design, water parcels were followed over several days, comparing
27 24 h in-situ measurements (^{14}C and $^{15}\text{NO}_3$, uptake, sediment trap export, dilution estimates of
28 phytoplankton growth and microzooplankton grazing) with high-resolution productivity
29 measurements by Fast Repetition Rate Fluorometry (FRRF) and Equilibrium Inlet Mass
30 Spectrometry (EIMS), and carbon export measured using sediment traps. Results show the
31 importance of accounting for temporal and fine spatial scale variability when estimating
32 ecosystem production. FRRF and EIMS measurements resolved diel patterns in gross primary
33 and net community production. Diel productivity changes agreed well with comparable more
34 traditional measurements. While differences in productivity metrics calculated over different
35 time intervals were considerable, as those methods rely on different base assumptions, the data
36 can be used to explain ecosystem processes which would otherwise have gone unnoticed. The
37 processes resolved from this method comparison further understanding of temporal and spatial
38 coupling and decoupling of surface productivity and potential carbon burial in a gradient from
39 coastal to offshore ecosystems.

40 **Plain Language Summary**

41 The California Current Ecosystem (CCE) is a site of coastal upwelling and is among the most
42 productive ecosystems in the world oceans, supporting fisheries of much of the western United
43 States, while playing a vital role in the economy of coastal communities. Accurately assessing
44 marine productivity in such regions is important for understanding the flux of carbon through the
45 food web and the ocean's ability to sequester carbon dioxide. Productivity assessments are,
46 however, often based on different methodologies relying on distinct cellular or ecosystem
47 assumptions. Each individual method can thus be misleading if its assumptions are not met,
48 while any single method is likely to fall short in terms of explaining ecosystem dynamics. Here,
49 we present a multi-method process-oriented investigation of diverse productivity methods in the
50 CCE Long-Term Ecological Research study region. Traditional 24 h in-situ incubation methods
51 were compared to high temporal resolution measurements using advanced optical and mass

52 spectrometric methods. The productivity rates and ecosystem processes resolved presented here
53 can help to further our understanding of the linkages between photosynthesis and respiration or
54 carbon production and sequestration. This approach can also help to improve productivity
55 assessments in complex ecosystems and to resolve the time-scales of these processes.

56 1. Introduction

57 Upwelling plays a key role in driving marine primary production along the eastern
58 continental margins of the world's oceans, making these ecosystems some of the most productive
59 regions in the world ([Chavez & Messie, 2009](#); [Dugdale, 1972](#); [Dunne et al., 2007](#); [Kudela et al.,](#)
60 [2008](#); [Longhurst et al., 1995](#); [Muller-Karger et al., 2005](#)). Upwelled water rich in inorganic
61 nutrients support intense phytoplankton blooms, typically dominated by large diatoms that
62 efficiently transfer newly produced biomass to higher trophic levels and into the mesopelagic via
63 sinking ([Kumar et al., 1995](#); [Michaels & Silver, 1988](#); [Stock & Dunne, 2010](#); [Thunell et al.,](#)
64 [2007](#)). Lateral transport also provides a significant flux of upwelled nutrients and coastal
65 planktonic communities to the offshore domain ([Nagai et al., 2015](#); [Plattner et al., 2005](#)),
66 resulting in complicated spatial and temporal connectivity between physical forcing, *in situ*
67 community composition and regional biogeochemistry.

68 While remote sensing techniques can reasonably quantify phytoplankton standing stocks
69 ([O'Reilly et al., 1998](#); [Saba et al., 2011](#)), primary production ([Behrenfeld & Falkowski, 1997](#);
70 [Kahru et al., 2015](#)), and even community composition ([Pan et al., 2011](#); [Uitz et al., 2015](#)), over
71 broad temporal and spatial scales, fine-scale and subsurface features remain challenging to
72 resolve from satellites. Shipboard incubation techniques allow more accurate measurements
73 throughout the photic zone, but cannot resolve highly spatially variable patterns in heterogenous
74 regions. In addition, shipboard methods with different assumptions, caveats and spatiotemporal
75 integration scales can be challenging to compare among cruises and regions. Consequently,
76 multi-method approaches for assessing productivity have proven useful for understanding the
77 nuances of processes that shape production responses to varying environmental conditions and
78 their relationships (e.g. [Hamme et al., 2012](#); [Quay et al., 2010](#); [Robinson et al., 2009](#); [Teeter et](#)
79 [al., 2018](#)).

80 Here, we take such a multi-method approach to reveal commonalities and complications
81 among several ecosystem production techniques applied to heterogeneous environmental settings

82 in the California Current Ecosystem (CCE) from coastal upwelling to the oligotrophic open
83 ocean. We especially want to emphasize that novel productivity assessment techniques can
84 reveal high temporal and spatial resolution of marine productivity which can in turn prove useful
85 in characterizing ecosystem productivity patterns. In the following section, we first touch briefly
86 on the various definitions and methods for assessing primary productivity and their issues. We
87 then describe process-oriented investigations on two field expeditions (spring 2016 and summer
88 2017; Fig. 1) in the CCE-LTER (Long Term Ecological Research) study region off of southern
89 California on which we compared traditional *in situ* measurements (^{14}C , $^{15}\text{NO}_3^-$, dilution-based
90 growth rates, and sediment traps) for assessing net primary production (NPP), new production
91 (NP) and export production to high-resolution production measurements of net carbon
92 production (NCP), O₂:Ar-based gross primary production (GPP) and FRRF-based
93 photophysiological measurements of GPP.

94 Two novel aspects of the study are highlighted. First, we utilized a Lagrangian approach,
95 tracking water parcels for several days, which allowed us to follow the evolution of production
96 processes during advective transport and to measure some aspects of diel variability. Second, we
97 field-tested and compared results for a new approach, described in detail in a companion paper
98 ([Wang et al., submitted](#)), that uses O₂/Ar to resolve temporal and spatial patterns of NCP in a
99 highly dynamic region. To our knowledge, this study comprises the first in-depth analysis of so
100 many different production assessments in a highly dynamic coastal setting. While some
101 differences are noted, as expected from the different processes measured, results from temporally
102 resolved production approaches are surprisingly consistent with traditional production
103 measurements, indicating that such approaches could provide important new insights into the
104 production dynamics of physically complex systems.

105 **2. Overview of Production Definitions and Measurement Approaches**

106 The many different techniques for assessing ocean production can be reasonably grouped in a
107 few broadly defined measurement categories. Gross Primary Production (GPP) is the rate of
108 organic carbon production by autotrophs. Net Primary Production (NPP) refers to GPP minus the
109 respiration performed by the autotrophs themselves. NPP thus accounts for both growth and
110 metabolic loss processes that lead to phytoplankton biomass production. The term New
111 Production (NP) refers to the portion of phytoplankton production based on the uptake of “new”

112 nitrogen (N) that enters the euphotic zone from external sources. NP sources include upwelled
113 NO_3^- , believed to be the dominant source of “new” nitrogen in the CCE, as well as nitrogen
114 delivered by atmospheric deposition, riverine input or nitrogen fixation. Export Production
115 measures the rate of carbon exported out of the euphotic zone where primary production occurs,
116 which is generally defined as the depth of penetration of 1% or 0.1% surface irradiance. Net
117 Community Production” (NCP), sometimes also called net ecosystem production, is defined as
118 GPP minus the respiration of all organisms in the ecosystem. As most production is eventually
119 respired at the community level, NCP rates need to be constrained by depth or time boundaries.
120 When integrated over appropriate spatial and temporal scales and converted to common units,
121 NCP, NP and export production should be in balance, representing the total amount of carbon or
122 nitrogen that can be exported from the euphotic zone by the biological carbon pump without
123 depleting biomass ([Eppley & Peterson, 1979](#)).

124 One of the most common methods for estimating primary production is the incorporation of
125 ^{14}C -labelled bicarbonate into particulate organic carbon ([Steemann Nielsen, 1952](#)). Although this
126 highly sensitive method has been a standard for aquatic production studies for decades,
127 interpretation is still highly debated ([Marra, 2009](#); [Peterson, 1980](#)). Measurements conducted
128 over a relatively short time approximate GPP, but longer incubations have increasing losses to
129 respiration. Experiment conducted over the full 24-h photocycle are thought to approach to NPP,
130 but should be underestimates because the respiratory losses include contributions from
131 heterotrophs that have consumed labelled C, in addition to respiration from autotrophs.
132 Interpretations are further complicated by starting incubations at different times of day, requiring
133 different weighting for uptake and respiration. Additionally, production can be significantly
134 underestimated when incorporation of ^{14}C into Dissolved Organic Carbon (DOC) is unmeasured
135 ([Laws et al., 2000](#); [Myklestad, 2000](#); [Teira et al., 2001](#)). NPP can also be assessed by the
136 seawater dilution method, where serial dilution is used to decouple growth and grazing
137 processes, allowing separate instantaneous rate estimates for phytoplankton growth and
138 microzooplankton grazing ([Landry & Hassett, 1982](#)). When carbon-based biomass estimates for
139 phytoplankton is combined with dilution-based daily rates, the calculated NPP result is the daily
140 net carbon biomass produced by phytoplankton absent losses that are a consequence of grazing
141 ([Barron et al., 2014](#); [Landry et al., 2000](#)).

142 The uptake and incorporation of $^{15}\text{NO}_3^-$ into phytoplankton cells can also be used to estimate
143 phytoplankton production derived from that nitrogen source ([Dugdale & Goering, 1967](#)). The
144 ^{15}N - NO_3^- method is thought to reduce the impact of internal elemental turnover, a process much
145 enhanced in the cellular carbon pool compared to cellular nitrogen. The measurement is based on
146 the enrichment of ^{15}N in cellular particulate organic nitrogen (PON) over the incubation period
147 and is defined as NP, under the assumption that nitrate is not regenerated from ammonium in the
148 euphotic zone. This method can, however, be impacted by processes such as ammonification or
149 nitrification in surface waters ([Yool et al., 2007](#)), which lead to under- or overestimates of NP. In
150 addition, luxury NO_3^- uptake ([Painter et al., 2007](#)) and release of previously fixed ^{15}N as DON
151 can also affect results of the ^{15}N method ([Bronk et al., 1994](#); [Collos, 1998](#)).

152 NCP, the balance between photosynthesis and community respiration, can be measured from
153 the oxygen budget of the ocean mixed layer. Because of the similar physical properties of O_2 and
154 Ar, NCP measurements based on the O_2/Ar method are mostly immune to mixed-layer physical
155 effects (e.g. solubility, gas exchange) on O_2 budgets over timescales of days to weeks. However,
156 coastal upwelling systems complicate the assumptions for this method ([Teeter et al., 2018](#)) since
157 such coastal water parcels exhibit a larger magnitude of short-term variations in productivity and
158 are subject to strong vertical fluxes that can alter surface O_2/Ar . Nonetheless, recent work has
159 shown that NCP can be applied on shorter timescales ([Hamme et al., 2012](#)) if the measurements
160 are conducted in a Lagrangian reference framework. Shortcomings of and improvements on this
161 method, which is used in our CCE method comparison, are discussed in detail in a companion
162 paper by ([Wang et al., submitted](#)).

163 Short-term measurements by the O_2/Ar method can also be used to estimate GPP if done in
164 the same Lagrangian-tracked water mass during the day (production + respiration) and night
165 (respiration) and assuming that nighttime respiration rate applies to the day. GPP is more
166 rigorously determined using isotopically labelled water (H_2^{18}O) ([Goldman et al., 2015](#)) or
167 oxygen ($^{18}\text{O}_2$) ([Kranz et al., 2010](#)) or from the natural isotopic composition of oxygen by the
168 $^{17}\Delta\text{O}_2$ triple O₂ isotope method ([Luz & Barkan, 2005](#)). However, these methods do not allow for
169 high-resolution spatiotemporal sampling and were not used here. Alternatively, the conversion
170 of sunlight into a biological redox potential in phytoplankton (i.e. electron generation at
171 photosystem II; PSII) can be assessed indirectly by variable fluorometry to provide another

172 nonintrusive PSII photochemical approach for estimating GPP at fine spatiotemporal scales.
173 Using the Single Turnover Method (STM) ([Falkowski & Kolber, 1993](#); [Kolber & Falkowski, 1993](#); [Moore et al., 2006](#); [Oxborough et al., 2012](#); [Suggett et al., 2001](#)) cellular energy allocation
174 between photochemical (energy generation and fixation of inorganic nutrients) and non-
175 photochemical (energy dissipation if excitation exceeds photochemical quenching) processes can
176 be quantified. However, the interpretation of the fluorescence signal is affected by environmental
177 conditions such as nutrient limitation, signal quenching under high-light intensities, as well as
178 other methodological sensitivities. Recent studies have recommended multiple improvements to
179 reduce uncertainties of the STM method ([Boatman et al., 2019](#); [Oxborough et al., 2012](#);
180 [Schuback & Tortell, 2019](#)), some of which we have applied in the present study. Most notably,
181 however, O₂:Ar-based NCP and GPP and variable fluorescence-based GPP approaches are
182 incubation-independent production measurements free from “bottle effects” and amenable to
183 flow-through applications that enable high spatiotemporal resolution sampling.

185

186 **3. Material and Methods**

187 **3.1 Cruise Background**

188 Production measurements were made during quasi-Lagrangian experiments conducted on
189 two Process cruises of the CCE LTER Program (Figure 1). The first cruise (RAPID CCE-LTER
190 cruise P1604, 19 April to 12 May 201, *R/V Sikuliaq*) investigated ecosystem responses during the
191 2015-2016 El Niño ([Jacox et al., 2016](#)) and had a wide geographic focus ranging from coastal
192 upwelling to oligotrophic offshore conditions ([Morrow et al., 2018](#); [Nickels & Ohman, 2018](#)).
193 The second cruise (P1706, 1 June to 2 July 2017, *R/V Roger Revelle*) followed community and
194 biogeochemical changes along a mesoscale filament transporting coastal waters to the offshore
195 domain. Experiments were thus conducted in a gradient ranging from newly upwelled water to
196 aged waters with a declining phytoplankton bloom. During both cruises, 3-4 quasi-Lagrangian
197 experiments (hereafter ‘cycles’) were conducted, yielding 7 total cycles. Cycles averaged ~3.5
198 days during which the cruise track followed a satellite-tracked Lagrangian drifter (Figure 1).
199 Deployment areas were first surveyed with a Moving Vessel Profiler (MVP) ([Ohman et al., 2012](#))
200 to ensure that they represented a cohesive water parcel free of strong frontal gradients. The
201 cycle was then initiated by deploying a sediment trap array followed by an array used for in situ
202 incubations ([Landry et al., 2012](#); [Stukel et al., 2013](#)). Both arrays had a 3×1-m holey sock drogue

203 centered at 15-m depth in the surface mixed layer and followed similar drift paths during the
204 cycles.

205 **3.2. Chlorophyll-a and Inorganic Nutrients**

206 During each day of a cycle, samples for chlorophyll and nutrients were taken with CTD
207 Niskin bottles at 8 depths spanning the photic zone. Chlorophyll-*a* was extracted following
208 [Strickland and Parsons \(1972\)](#). A more detailed description of sample analysis can be found in
209 the supplemental materials (S-M 1). Nutrient samples were filtered using a 0.1 μ m Acropak filter
210 prior to freezing for shore-based analysis. Dissolved inorganic nutrients (nitrate, nitrite, silicate,
211 phosphate and ammonium) were analyzed using an automated flow injection autoanalyzer on a
212 Lachat Instruments QuikChem 8000 ([Gordon et al., 1992](#)). The precision of these measurements
213 was $\pm 5\%$, and the detection levels for nitrate + nitrite, nitrite, ammonium, phosphate and silicate
214 were 0.2, 0.1, 0.1, 0.1 and 1.0 μ M, respectively.

215 **3.3. Bottle incubations: ^{14}C Net Primary Production (NPP_{14C}) and $^{15}\text{NO}_3^-$ New Production
216 (NP)**

217 ^{14}C Net Primary Production (NPP_{14C}) and $^{15}\text{NO}_3^-$ -based New Production (NP) were quantified
218 from *in situ* incubations for each day of the cycles at 6 depths spanning the euphotic zone. Niskin
219 bottle samples were gently transferred to polycarbonate incubation bottles (triplicate 250-mL
220 bottles plus a dark bottle for NPP_{14C} and a single 1-L bottle for NP) using silicon tubing. Samples
221 were then spiked with H $^{14}\text{CO}_3^-$ (NPP_{14C}) or K $^{15}\text{NO}_3^-$ (NP) and incubated for 24 h in mesh bags
222 hung below the drift array. Incubations were started and terminated at \sim 04:00 local time. NPP_{14C}
223 samples were then filtered onto GF/F filters, acidified for 24 h (0.5 ml of 10% biological grade
224 HCl), placed in scintillation cocktail, and subsequently counted using a liquid scintillation
225 counter (details in ([Morrow et al., 2018](#))). NP samples were filtered onto GF/F filters and frozen
226 at sea. On land, they were acidified (fumed concentrated (37%) HCl), dried, and analyzed by
227 isotope ratio mass spectrometry at the UC Davis Analytical Facility. Nitrate uptake was
228 calculated following ([Dugdale & Wilkerson, 1986](#)) with a slight modification similar to ρ_{is} in
229 ([Kanda et al., 2003](#)) when the nitrate spike was $>10\%$ of ambient nitrate ([Stukel et al., 2016](#)). On
230 the P1706 cruise, NPP_{14C} samples were lost and NPP_{14C} was estimated using an algorithm fitted
231 to CCE NPP_{14C} data, as described below.

232 **3.4. Net Production Estimates based on Chlorophyll, Light and Nutrients**

233 For the P1706 cruise, we estimated NPP rates from ambient light, nutrients, and Chl *a* as
234 described by ([Stukel et al., 2019a](#)). The initial algorithm was developed using irradiance to
235 predict Chl *a* specific production ([Morrow et al., 2018](#)) and then adapted for general use in the
236 CCE. The algorithm was parameterized from data collected on seven previous CCE-LTER
237 process cruises for which ^{14}C -PP data were available. P1706 NPP was subsequently calculated
238 as:

239
$$\frac{\text{NPP}}{\text{Chl}} = V_{0m} \cdot (1 - e^{(-\alpha \cdot \text{PAR}/V_{0m})}) \cdot \frac{NH_4}{NH_4 + K_S} \quad (\text{Eq. 1})$$

240 where NPP/Chl is the chlorophyll-specific primary production in units of mg C d⁻¹ (mg Chl)⁻¹,
241 PAR is average daily photosynthetically active radiation (units of $\mu\text{mol photons m}^{-2} \text{s}^{-1}$) within
242 the mixed layer, $(1 - \exp(-\alpha \cdot \text{PAR}/V_{0m}))$ describes the light saturation and inhibition term
243 with $V_{0m} = 66.5 \text{ mg C d}^{-1} (\text{mg Chl})^{-1}$ and $\alpha = 1.5$; and $\frac{NH_4}{NH_4 + K_S}$ describes the ammonium-limitation
244 kinetics with $K_S = 0.025 \mu\text{mol L}^{-1}$. Uncertainties in the algorithm were propagated through all
245 subsequent equations following ([Stukel et al., 2019a](#)) When averaged over the duration of a
246 cycle, propagated errors in mixed layer NPP were $\pm 30 - 40\%$ at the 95% confidence limit.

247 **3.5 Net Phytoplankton Production from Dilution Experiments (NPP_{G:G})**

248 To calculate phytoplankton intrinsic growth rates and microzooplankton grazing rates,
249 dilution experiments were prepared following the two-treatment dilution approach ([Landry et al.,](#)
250 [2008](#); [Landry et al., 2011b](#); [Stukel et al., 2012](#)). Each experiment consisted of water collected at
251 6 depths spanning the euphotic zone (i.e. “array depths”) in pre-dawn CTD casts (02:00 local).
252 At each depth, two 2.7 L polycarbonate bottles were filled with either unfiltered seawater (i.e.
253 100% whole seawater) or a mixture of 33% whole seawater and 67% 0.1- μm filtered seawater.
254 Samples were incubated in situ on the drifter array for 24 h along with the NPP_{14C} and NP
255 experiments. Net growth rates in each bottle were determined from changes in fluorometrically-
256 measured Chl *a* and used to quantify gross growth rates (μ) and mortality due to protistan grazing
257 (m). Carbon to Chl *a* ratios (C:Chl) were determined using the approach of [Li et al. \(2010\)](#), based
258 on microscopy-derived estimates of phytoplankton biomass in the CCE region. C:Chl was

259 multiplied by Chl to determine initial carbon biomass (B_0), and phytoplankton production was
260 calculated as $NPP_{G:G} = \mu B_0 e^{\mu-m}/(\mu - m)$, following [Landry et al. \(2016\)](#).

261 **3.6. Net and Gross Community Production from O₂/Ar Measurements (NCP; GPP_{O₂/Ar})**

262 Continuous samples of dissolved O₂/Ar were taken from the ship's underway seawater
263 system. O₂/Ar gas ratios were measured with a Pfeiffer QMC 200 mass spectrometer equipped
264 with an equilibration inlet (EIMS) ([Cassar et al., 2009](#)). Temperature and oxygen concentrations
265 were measured using Aandera temperature sensors (model 3835) and oxygen optodes. The signal
266 was filtered to within an 8 km distance between the ship and the drifter (e.g. removing values
267 during plankton net tows when the ship was far from the drifter location), and calibration and
268 maintenance times were also removed. Net rates of community production (NCP) from O₂/Ar
269 measurements reflect oxygen production by photoautotrophs, respiration by photo- and
270 heterotrophs and corrections for physical gas exchange processes. NCP rates are calculated for
271 the mixed layer depth (MLD) assuming no advective fluxes of O₂/Ar from neighboring water
272 parcels and represent processes occurring over the residence time of O₂ assuming a steady state
273 system:

274
$$NCP_{prior} = k \cdot \Delta(O_2/Ar)[O_2]_{sol}\rho \quad (\text{Eq. 2})$$

275 NCP_{prior} estimates the time-averaged NCP based on wind speed history, MLD, and the
276 observed biological oxygen signal, where k is the time-weighted piston velocity ([see Reuer et al.,](#)
277 [2007](#)) incorporating the wind speed history and MLD. $[O_2]_{sol}$ is the mixed layer oxygen
278 solubility, and ρ is the average density of the mixed layer. $\Delta(O_2/Ar)$ is the biological oxygen
279 signal defined by $\Delta(O_2/Ar) = \frac{(O_2/Ar)}{(O_2/Ar)_{cal}} - 1$. Due to our Lagrangian study design, we were able
280 to measure short-term changes in mixed layer $\Delta(O_2/Ar)$ in real time (“instantaneous changes”)
281 and thereby estimate NCP over shorter timescales than the residence time of mixed layer O₂ (see
282 [Hamme et al., 2012](#); [Teeter et al., 2018](#); [Wang et al., submitted](#)).

283
$$NCP_{inst} = z \frac{\Delta(\Delta(O_2/Ar))}{\Delta t} [O_2]_{sol}\rho + \bar{k}(\Delta O_2/Ar)[O_2]_{sol}\rho \quad (\text{Eq. 3})$$

284 where z denotes MLD and \bar{k} represents the instantaneous gas exchange coefficient averaged over
285 the preceding hour (i.e. Δt). Using community respiration measured during the night,
286 NCP_(inst,night) & assuming similar day and night respiration, GPP can be estimated as:

$$287 \quad GPP_{NCP} = NCP_{inst,day} - NCP_{inst,night} \quad (\text{Eq. 4})$$

288 3.7. Estimating Mixed-Layer GPP using FRRF

In addition to the O₂/Ar method, we also estimated GPP independently on the P1706 cruise based on the photo-physiology of the mixed-layer phytoplankton community measured by FRRF. Shipboard measurements were made using a bench-top FastAct 2+ Fast TRAKA instrument (Chelsea, UK) plumbed into the ship's running seawater system. Photosynthesis versus irradiance (P vs. E) curves were run continuously on a ~45 min sampling interval. Using a modified version of the absorbance algorithm following [Oxborough et al. \(2012\)](#), volume-based productivity rates (i.e. mol electrons (RCII)⁻¹ m⁻³ d⁻¹) are calculated as:

$$J_{V_{PSII,abs}} = \Phi_{RCII} \cdot F'_o \cdot K_a \cdot E \cdot 8.64 \times 10^{-8} \quad (\text{Eq. 5})$$

where $F'_o = (F_m \cdot F_0) / (F_m - F_0) \cdot (F'_q/F_m)$. $K_a = 11800 \text{ m}^{-1}$ is an instrument-specific calibration factor, E = irradiance ($\mu\text{mol photons m}^{-2} \text{ s}^{-1}$), the factor 8.64×10^{-8} converts $\mu\text{mol photons m}^{-2} \text{ s}^{-1}$ to mol photons $\text{m}^{-2} \text{ d}^{-1}$ and kg/m^{-3} to mg/m^{-3} . The parameter Φ_{RCII} (mol e^- mol photon $^{-1}$) has a constant value of 1, representing one electron transferred from P680 to quinone A (Q_A) for each photon absorbed and delivered a reaction center (RCII) ([Kolber & Falkowski, 1993](#)). RCII was estimated as:

$$RCII = K_a \cdot \frac{F_0}{\sigma_{PSII}} \quad (\text{Eq. 6})$$

where F_0 is dark-adapted base fluorescence and σ_{PSII} is the absorption cross-section area of the photosystem. As the RCII estimate might be biased by base fluorescence quenching during daytime, JV_{PSII} was corrected using an average RCII estimate from nighttime measurements (01:00 – 05:00 local). JV_{PSII} ($\text{mol electrons m}^{-3} \text{ d}^{-1}$) was converted to carbon units using the conversion factor $\Phi_{e:c}$ ([Schuback & Tortell, 2019](#)):

$$309 \quad \Phi_{e:c} / \eta_{RCII} = 486 \cdot NPQ_{NSV} + 1854 \quad (\text{Eq. 7})$$

310 where $\Phi_{e:C}$ is the electron generation to carbon fixation ratio, η_{RCII} is the RCII to Chl- a ratio and
 311 NPQ_{NSV} is the normalized Stern-Volmer non-photochemical quenching coefficient. Since
 312 NPQ_{NSV} changed throughout the water column with changing light intensities, $\Phi_{e:C}$ was variable.
 313 For simplicity, we used a literature value of 0.003 for η_{RCII} ([Lawrenz et al., 2013](#)) but
 314 recommend that η_{RCII} be measured directly on future cruises to avoid biasing estimates of $\Phi_{e:C}$.

315 More detailed descriptions of the measured and calculated parameters and additional information
316 for the production estimates using FRRF are provided in the supplemental material (Table S1).

317 To calculate mixed-layer GPP from FRRF measurements, we used the *in situ* light
318 attenuation from the CTD profile around noon to calculate the light field in the mixed layer over
319 the diurnal cycle. The time-varying *in situ* light field was modeled using the empirical
320 transmission-light attenuation relationship and surface photosynthetically active radiation (PAR)
321 measured by the ship's meteorological system. Photosynthesis vs. irradiance relationships were
322 determined by fitting the productivity rate estimates from the FRRF versus the irradiance from
323 the FRRF light curves using the [Platt et al. \(1980\)](#) definition:

324
$$\text{Productivity} = Ps \times [1 - e^{\frac{-\alpha \times E}{Ps}}] \times e^{\frac{-\beta \times E}{Ps}}$$
 (Eq. 8)

325 where Ps equals the maximum photosynthesis, E equals is the irradiance (PAR), α is the initial
326 slope of photosynthesis under low irradiance and β is the slope under high/stressful irradiance.
327 Additional methods on photophysiology including a table with the nomenclature is available in
328 the supplemental material (methods S1 and Table S1).

329 **3.8. Sediment Trap Deployments**

330 We deployed VERTEX-style surface-tethered drifting sediment traps ([Knauer et al., 1979](#))
331 near the base of the euphotic zone. Trap crosspieces holding 12 acrylic tubes with an 8:1 aspect
332 ratio, topped with baffles constructed of smaller beveled tubes, were deployed on a line with
333 surface floats and a holey-sock drogue centered at 15-m depth. Tubes were deployed with a
334 saltwater brine of filtered seawater and 0.4% formaldehyde. After recovery, overlying seawater
335 was removed by gentle suction, and samples were analyzed under a dissecting microscope to
336 remove mesozooplankton 'swimmers'. Samples were then split on a Folsom splitter, filtered onto
337 pre-combusted GF/F filters, acidified and analyzed for C, N, and isotopes on an isotope ratio
338 mass spectrometer at the UC Davis Stable Isotope Facility. Previous comparisons with
339 independent export flux estimates made using ^{238}U - ^{234}Th disequilibrium approaches have shown
340 no substantial over- or under-collection biases for our sediment trap configuration in the CCE
341 ([Stukel et al., 2019](#)). For additional deployment and processing details, [see Stukel et al. \(2019b\)](#).

342 **3.9. Statistics**

343 For all cycle data, variability was quantified as the standard errors of the means using the
344 available 24-hour integrated data. Since intra-cycle variability was a combination of
345 measurement uncertainty and ecosystem variability, standard parametric statistics were not
346 applicable. Throughout this manuscript, we present vertically integrated rates throughout the
347 mixed layer, unless otherwise stated. For bottle samples, we used trapezoidal integration. For the
348 NPP_{14C} algorithm used for the P1706 cruise, uncertainties in parameter estimates were
349 propagated through all equations.

350 **4. Results**

351 **4.1. General Features of the Two Cruises**

352 Four different regions were sampled during the P1604 cruise (Figure 1): the offshore
353 stratified region (P1604-C1), the core of the California Current (P1604-C2), offshore of the
354 coastal boundary in the wind stress curl upwelling domain (P1604-C3), and the coastal boundary
355 upwelling region (P1604-C4). Over the course of 4 cycles on P1706, we followed upwelled
356 waters from nearshore to offshore. P1706-C1 was located in freshly upwelled waters; P1706-C2
357 started ~77 km NW of the end of P1706-C1 in partially aged upwelled waters; and P1706-C3
358 began ~140 km southwest of the start of P1706-C2 in post-bloom waters. Post-cruise analysis
359 indicated that P1706-C3 was not part of the main filament and contained water characteristic of
360 the California Current, likely advected from the North. P1706-C4 was a continuation of P1706-
361 C2 initiated about 26 km northeast of the start of P1706-C3 (Figure 1). Average mixed-layer
362 depth, temperature, Chl *a*, nutrient concentrations are given in Table S2 for all cycles. Full data
363 are available in the CCE-LTER database:

364 https://oceaninformatics.ucsd.edu/databooz/catalogs/ccelter/datasets?fc=11:29820&ps=1:0_2:0_3:0_9:0_11:0.

366 **4.2. Phytoplankton Production**

367 **4.2.1. ¹⁴C Primary Production**

368 ¹⁴C-derived estimates of NPP are from field incubations conducted during P1604 and from a
369 general algorithm based on CCE field incubations for P1706 (Stukel et al. 2019). Both are
370 defined as NPP_{14C} and treated the same.

371 NPP_{14C} decreased slightly between successive days during P1604-C2 (22, 17 and 14 mmol C
372 m⁻² d⁻¹), increased daily during P1604-C3 (36, 45 and 64 mmol C m⁻² d⁻¹), and had the highest
373 rates (150, 103 and 113 mmol C m⁻² d⁻¹) during P1604-C4 (Fig. 3, Table S4). A strong gradient
374 of decreasing NPP_{14C} with distance from shore is therefore evident in the P1604 data.

375 NPP_{14C} for P1706 showed a wider range of results but a similar decrease from nearshore to
376 offshore (Fig. 4, Table S4). In freshly upwelled waters during P1706-C1, production tripled from
377 220 mmol C m⁻² d⁻¹ for day 1 (D1) to 718 and 596 mmol C m⁻² d⁻¹ for D2 and D3, respectively.
378 In P1706-C4 offshore waters, average NPP_{14C} was 30-fold lower (13 and 19 mmol C m⁻² d⁻¹ for
379 D1 and D2, respectively). Between these extremes, NPP_{14C} varied from ~250 to 300 mmol C m⁻²
380 d⁻¹ during P1706-C2 and decreased from ~90 to 48 mmol C m⁻² d⁻¹ from D1 to D3 during P1706-
381 C3.

382 **4.2.2. *NPP_{G/G} from Dilution Growth and Grazing Rates***

383 NPP_{G/G} estimates closely follow the magnitudes and trends observed for NPP_{14C} (Table 1).
384 Mean rates are higher for P1604-C3 compared to C2 (48.4 ± 8.4 vs 17.7 ± 4.5 mmol C m⁻² d⁻¹)
385 and decrease even further to 9.4 mmol C m⁻² d⁻¹ during P1604-C1. For P1604-C2, day-to-day
386 NPP_{G/G} variability (44, 24 and 36 mmol C m⁻² d⁻¹ for D1-D3, respectively), is similar to that of
387 NP and NPP measurements. During P1604-C3, NPP_{G/G} increased from 49 to 76 mmol C m⁻² d⁻¹
388 over the 3-day occupation, similar to the increase in independently measured NPP_{14C}. While no
389 NPP_{G/G} data were obtained for the nearshore P1604-C4, the high rates were found in the freshly
390 upwelled waters of P1706-C1 (511 ± 150 mmol C m⁻² d⁻¹; range 252 to 588 mmol C m⁻² d⁻¹).
391 Over subsequent P1706 experiments, NPP_{G/G} decreased each day along the upwelling filament,
392 averaging 270 ± 44 , 76 ± 39 and 22 ± 6 mmol C m⁻² d⁻¹ for cycles 2 to 4, respectively.

393 **3.2.3: *New production (¹⁵NO₃ uptake)***

394 Mixed-layer integrated rates of nitrate-based new production (NP) are given in Table 1 as
395 carbon equivalents using a N:C conversion of 6.625. For P1604, mean NP rates of 11 ± 3 mmol
396 C m⁻² d⁻¹ during offshore cycle 2 increased to 24 ± 8 and 23 ± 6 mmol C m⁻² d⁻¹, respectively,
397 during cycles 3 and 4. For P1706, NP was highest (157 ± 19 mmol C m⁻² d⁻¹) in C1 upwelled
398 waters, and declined progressively during offshore filament transport. NP averaged 101 ± 44
399 mmol C m⁻² d⁻¹ during P1706-C2, but decreased by 75% from days D1 and D2 to D3 (Table S4).

400 Further offshore, NP decreased to 29 ± 18 and 5 ± 0.1 mmol C m $^{-2}$ d $^{-1}$ during C3 and C4,
401 respectively. *f*-ratios (the ratio of new to total production, estimated as NP/NPP $_{14C}$) varied from
402 0.2 to 0.7 over all experiments but lacked a consistent onshore-offshore trend (Table 1).

403 **3.2.4: Net community Production (NCP_{prior})**

404 Conventional O₂/Ar-NCP estimates in complex systems such as the CCE are challenging to
405 interpret. Our companion paper ([Wang et al., submitted](#)) discusses these shortcomings along with
406 method improvements used to estimate NCP more reliably in the present field campaigns. Here,
407 we use these new insights in discussing the traditional NCP analysis (NCP_{prior}) and a real-time
408 NCP (NCP_{inst}), which integrate O₂/Ar signals over different time scales. The O₂ residence time,
409 as determined by wind-speed reanalysis and mixed layer depth was between 6.6 and 15.6 days
410 for P1604 and between 2.6 and 9.0 days for P1706 ([Wang et al., submitted](#)). During both cruises,
411 the heterogenous nature of NCP in the CCE-LTER region is indicated by significant short- and
412 long-term trends in NCP_{prior} (Figs. 3, 4).

413 NCP_{prior} was steady and low during P1604-C2 and highest during P1694-C4 (5.5 ± 0.3 and
414 39.5 ± 4.0 mmol C m $^{-2}$ d $^{-1}$, respectively; Table 1). Although the water mass appeared well
415 equilibrated with the atmosphere during P1604-C3, NCP_{prior} changed from slightly net
416 heterotrophic at the beginning of the cycle (-10.7 mmol C m $^{-2}$ d $^{-1}$) to slightly net autotrophic (8.6
417 mmol C m $^{-2}$ d $^{-1}$) at the end, averaging -0.3 ± 5.6 mmol C m $^{-2}$ d $^{-1}$. NCP_{prior} showed clear diurnal
418 amplitudes during P1604-C2 and C4, with increasing rates during daylight and decreasing rates
419 at night (Fig. 3). The diurnal amplitude was, however, less pronounced during P1604-C3.

420 **4.2.5. Real-time Analysis of NCP (NCP_{inst})**

421 Real-time analysis of NCP data (NCP_{inst}) accounts mainly for O₂/Ar change over the
422 previous 1 hour, including the instantaneous gas exchange coefficients. The system was net
423 autotrophic for P1604-C2 and C4, decreasing from 9.7 to 1.1 mmol C m $^{-2}$ d $^{-1}$ over the duration of
424 C2 (Table S4) and subsequently increasing to 16.4 ± 4.0 mmol C m $^{-2}$ d $^{-1}$ for C4 (Tables 2 and
425 S4). NCP_{inst} indicates a slightly net heterotrophic system (-0.1 ± 1.2 mmol C m $^{-2}$ d $^{-1}$) during
426 P1604-C3.

427 NCP_{inst} estimates were net autotrophic for P1706-C1 (77.8 ± 0.5 mmol C m $^{-2}$ d $^{-1}$) and net
428 heterotrophic for P1706-C2 (-14.3 ± 11.3 mmol C m $^{-2}$ d $^{-1}$). For cycles 3 and 4, the signals were

429 strongly affected by ship movements through other waters mixed in with the relatively narrow
430 filament. Consequently, we view these NCP_{RT} estimates as unreliable and do not discuss them
431 further.

432 **4.2.6 Gross Primary Production based on NCP ($GPP_{O_2/Ar}$)**

433 $GPP_{O_2/Ar}$ averaged 42 ± 9 and ~ 130 mmol C m⁻² d⁻¹ for P1604-C2 and C3, respectively. No
434 error determination could be made for C3 as the respiration measurements during days 1 and 2
435 were positive values when the ship moved through different water masses; hence, only day 3
436 date could be used for this cycle. High $GPP_{O_2/Ar}$ rates were estimated for nearshore cycles P1604-
437 C4 (4348 ± 171 mmol C m⁻² d⁻¹) and P1706-C1 (1082 ± 134 mmol C m⁻² d⁻¹). For P1706-C2,
438 estimated GPP declined to 401 ± 52 mmol C m⁻² d⁻¹. As noted above, estimates for P1706-C3 and
439 C4 were compromised by ship movements through mixed waters.

440 **4.2.7. GPP_{FRRF} Estimates**

441 No FRRF measurements were conducted during P1604. For P1706, mean GPP_{FRRF} estimates
442 declined progressively following along onshore-to-offshore filament transport of upwelled water
443 from 762 ± 148 to 502 ± 92.8 $\mu\text{g C m}^{-2} \text{d}^{-1}$ for C1 and C2, respectively, to 92.4 ± 13 and 31 ± 1
444 $\mu\text{g C m}^{-2} \text{d}^{-1}$, for C3 and C4 (Fig. 4F, Table 1). For P1706-C1, diurnally averaged GPP increased
445 with time spent in the water mass (519 to 1148 $\mu\text{g C m}^{-2} \text{d}^{-1}$ for D1 to D3; Table S4). For other
446 P1706 cycles, GPP was relatively constant or decreased slightly (Table S4). As shown in Fig. 4,
447 GPP rates showed a distinct diurnal periodicity with notably higher rates during the
448 noon/afternoon hours. Spikes during P1706-C1 and C2 are most associated with occasional net
449 tows when the ship briefly left the drift array and entered water parcels with higher surface Chl
450 *a*.

451 **4.3. Photophysiology and Light Acclimation**

452 The maximum quantum yield (F_v/F_m) of the dark-adapted phytoplankton community for
453 P1706-C1 was around 0.48 to 0.5 during nighttime and morning hours but dipped to ~ 0.4 at the
454 end of the photoperiod of D2 and D3 (Fig. S1). Values of ~ 0.5 are the maximum measurable in
455 non-stressed cells using single turnover measurements with our FRRF instrument. For P1706-
456 C2, F_v/F_m was lower (0.39-0.42) during night and morning hours, but also showed a relative
457 decline towards the end of each photoperiod. F_v/F_m increased steadily from 0.4 to ~ 0.49 during

458 P1706-C3 but was relatively constant (~0.45) for P1706-C4. Both of these cycles (C3 and C4)
459 were dominated by smaller phytoplankton, mainly cyanobacteria, and neither displayed the
460 distinct diel decreases in Fv/Fm as seen in C1 and C2. The absorption cross sectional area of
461 PSII (σ), did not show a diel pattern, yet, σ was enhanced during C2 ($6 \text{ nm}^2 \text{ PSII}^{-1}$) compared to
462 C1 ($4 - 5 \text{ nm}^2 \text{ PSII}^{-1}$). For C3, σ was $6 \text{ nm}^2 \text{ PSII}^{-1}$ while in C4 the absorption cross sectional area
463 of PSII was $5.5 \text{ nm}^2 \text{ PSII}^{-1}$. $1/\tau$ decreased throughout the light phase and increased during the
464 dark period. This pattern was well defined in C1 and C2, damped in C3 and non-existent in
465 C4. Compared to C1, $1/\tau$ increased in our C2 measurements. Enhanced NPQ_{NSV} rates (data not
466 shown) were also measured in C2. Parameters derived from the fluorescence induction curves
467 (α , P_{\max}) showed some variability within and between cycles. Maximum photosynthetic electron
468 transport (P_{\max}) increased towards the ends of each photoperiod in C1 and C2, but was relatively
469 constant for C3 and C4 (Fig. S1). α did not show diel changes, yet, values for C1 and C2 were
470 significantly lower compared to C3 and C4. The light saturation point (E_K) (averages, including
471 light and dark phase, were 427 ± 106 for C1, 389 ± 203 for C2, 555 ± 143 for C3 and 583 ± 133
472 for C4). Those values are much higher than mean mixed-layer daytime light intensities, which
473 averaged 151, 170, 140, and $329 \mu\text{mol photons m}^{-2} \text{s}^{-1}$ for C1-C4, respectively. Light intensity
474 and E_K were not correlated. Similarly, no change in the initial slope (α) was observed with
475 changes in mean daytime light intensity.

476 4.4. Export Flux

477 Sediment trap-measured export near the base of the euphotic zone decreased with distance
478 from shore on the P1604 cruise, with values of 20.9 , 10.0 and $3.4 \text{ mmol C m}^{-2} \text{ d}^{-1}$ for coastal C4,
479 transition C3, and offshore C2, respectively (Fig. 3). Export efficiency, however, remained
480 relatively constant with distance from shore on this cruise. The *e*-ratio (defined as
481 export/NPP_{14C,eup}, where NPP_{14C,eup} is NPP_{14C} integrated to the base of the euphotic zone) was
482 0.15, 0.14 and 0.15 for C2–C4, respectively. In contrast, export near the base of the euphotic
483 zone showed no clear trend with distance from shore on P1706. Sinking flux was 29.3 mmol C
484 $\text{m}^{-2} \text{ d}^{-1}$ in the coastal C1, $44.5 \text{ mmol C m}^{-2} \text{ d}^{-1}$ in the early filament C2, $35.7 \text{ mmol C m}^{-2} \text{ d}^{-1}$ in
485 the late filament C4, and $46.7 \text{ mmol C m}^{-2} \text{ d}^{-1}$ in transition water C3 (Fig. 4). This led to an
486 inverse relationship between mixed-layer Chl a and the *e*-ratio, with *e*-ratios of 0.05 , 0.18 , 0.43
487 and 0.79 for C1–C4, respectively.

488 **4.5. Inter- and Intra-cruise Variability in Production Relationships**

489 Cycle P1604-C2 started in the core of the California Current, and new production was
490 matched by modest NCP values and a diel pattern in the dO₂/Ar measurements (Fig 3 J,L).
491 Overall, P1604-C2 was moderately net autotrophic but, due to the partial depletion of nutrients
492 and change in weather conditions, most production measures showed reduced rates toward the
493 end of the cycle. For P1604-C3, offshore of the coastal boundary in the wind stress curl
494 upwelling domain, NPP and new production-based estimates increased significantly compared to
495 C2, yet NCP_{prior} was negative at the beginning of the cycle, but became positive around D3. This
496 change in production was correlated with a change in weather as the sea became much calmer
497 and cloud cover was reduced. As expected, productivity was highest in the coastal upwelling
498 region (P1604-C4), where carbon-based production rates tripled. Despite high NO₃⁻
499 concentrations, the phytoplankton appeared to utilized NH₄⁺ primarily for growth. NCP_{prior}
500 during P1604 indicated that the system was strongly net autotrophic.

501 Productivity was high where nutrients were plentiful close to shore in the freshly upwelled
502 water of P1706-C1. However, overcast light conditions reduced productivity estimates (except
503 NCP_{prior}) during the early part of this cycle. Comparatively low NP:NPP rate estimates indicate
504 that the phytoplankton community used both ammonia and nitrate as N sources. NCP_{prior} rates
505 averaged 50% of NP, but a distinct diel pattern was observed. P1706-C2 showed reduced
506 production compared to C1, as a result of reduced chlorophyll concentration. Despite lower NPP,
507 NP was higher on day one of C2 compared to C1. NCP analysis indicated that the watermass
508 started to become net heterotrophic at the end of this cycle. P1706-C3 was conducted in a region
509 just outside of the filament where water from the California Current mixed with filament water.
510 P1706-C3 was initially net autotrophic, but production rates were strongly reduced compared to
511 C1 and C2 . The continuous negative trend in NCP was likely driven by horizontal and vertical
512 mixing of different water masses, a deepening of the mixed layer depth over time and the
513 observed decrease of Chl a during this cycle. P1704-C4 was conducted at the location of a drifter
514 that marked the water parcel sampled during C2 and can thus be considered an extension of the
515 previous filament cycle. It was characterized by low chlorophyll despite a nitrate concentration
516 of around 2.9 μM and an ammonium concentration of 1.7 μM. The extremely low NP and the
517 low f-ratio (0.24) also indicate that the phytoplankton community was taking up mostly
518 regenerated N. Further analysis (see discussion below) indicated that cycle 2 was iron limited.

519 NCP rates were found to be near air saturation, indicating that autotrophic and heterotrophic
520 processes were in balance despite the elevated ammonium.

521 **4.5. Production Comparison**

522 We had two independent estimates of GPP (GPP_{FRRF} and $\text{GPP}_{\text{O}_2/\text{Ar}}$), two independent
523 estimates of NPP ($\text{NPP}_{14\text{C}}$ and $\text{NPP}_{\text{G}/\text{G}}$), and three estimates of NCP or NP ($\text{NCP}_{\text{prior}}$, NCP_{RT} , and
524 nitrate uptake). The independent GPP experiments can only be compared for two cycles (P1706-
525 C1 and P1706-C2) because FRRF measurements were not made on the P1604 cruise and because
526 ship movements in and out of the mesoscale filament invalidated $\text{GPP}_{\text{O}_2/\text{Ar}}$ assumptions for
527 P1706-C3 and C4. Nonetheless, there is reasonable agreement between the two methods. On
528 P1706-C1, the ratio of $\text{GPP}_{\text{FRRF}}:\text{GPP}_{\text{O}_2\text{Ar}}$ was 0.75, and on P1706-C2 it was 1.25. Agreement
529 was even better for the two NPP measurements, yielding a Pearson's linear correlation of 0.9997
530 ($p < 10^{-5}$). The mean $\text{NPP}_{14\text{C}}$ across all paired cycles was $214 \text{ mmol C m}^{-2} \text{ d}^{-1}$, while the mean
531 $\text{NPP}_{\text{G}/\text{G}}$ was $223 \text{ mmol C m}^{-2} \text{ d}^{-1}$. Comparing mean NPPs to mean GPPs for P1706-C1 and C2
532 (941 and $465 \text{ mmol C m}^{-2} \text{ d}^{-1}$ for C1 and C2, respectively), the resulting NPP:GPP ratios are 0.55
533 and 0.56 , respectively, suggesting that 55% of phytoplankton GPP, on average, goes to biomass
534 production. Compared to the agreement between alternate GPP or NPP measurements, the
535 correlation between $\text{NCP}_{\text{prior}}$ and NCP_{inst} is weak and not statistically significant (Pearson's $\rho =$
536 0.60 , $p = 0.15$). This discrepancy was expected, however, as it reflects the different temporal
537 integration scales of $\text{NCP}_{\text{prior}}$ and NCP_{inst} and the substantial differences in NCP observed in the
538 P1706 filament. There is also substantial discrepancy between NP and the two NCP estimates.
539 The strongest correlation is between NP and $\text{NCP}_{\text{prior}}$, though not statistically significant ($\rho =$
540 0.52 , $p = 0.24$). NP measurements also substantially exceed those of $\text{NCP}_{\text{prior}}$ and NCP_{RT} , where
541 mean $\text{NCP}_{\text{prior}}$ is $8.7 \text{ mmol C m}^{-2} \text{ d}^{-1}$ and mean NP is $73 \text{ mmol C m}^{-2} \text{ d}^{-1}$.

542 **5. Discussion**

543 The P1604 and P1706 cruises both aimed to measure ecosystem dynamics and
544 biogeochemical rates. The Lagrangian sampling plan and multi-method approach allowed us to
545 compare a number of different productivity estimates over a broad range of environmental
546 conditions. P1604 occurred near the end of an anomalously warm period in the northeast Pacific
547 that began with the 2014-2015 North Pacific heat wave and continued with an El Niño in 2015-

548 2016 ([Bond et al., 2015](#); [Jacox et al., 2016](#)). At the time of this cruise, much of the region
549 remained above normal temperatures, but upwelling had resumed along the coast, leading to
550 phytoplankton blooms during nearshore experiments P1604-C3 and C4. P1706 aimed to follow
551 filament transport of freshly upwelled water offshore. Due to this mesoscale focus, P1706 cruise
552 results are substantially influenced by: 1) rapid changes in water column properties over time; 2)
553 mixing of upwelled and offshore waters during transport; and 3) small-scale spatial gradients in
554 the vicinity of the drift array. In the following discussion, we consider the compatibility and
555 differences among multiple primary production measurements and their applicability in this
556 dynamic region. To compare productivity rate estimates, all data are integrated over the same
557 temporal scale (24 h, cycle duration), analyzed over the mixed layer depth and normalized to
558 carbon units.

559 **5.1. GPP_{FRRF} and GPP_{O₂/Ar} Comparisons to NPP**

560 Only recently has it been possible to measure GPP rates with high temporal resolution during
561 research cruises ([Hamme et al., 2012](#); [Schuback & Tortell, 2019](#)). Here, we used GPP estimates
562 based on underway FRRF measurements and rates derived from O₂/Ar data. We modified the
563 FRRF method described by [Oxborough et al. \(2012\)](#) to account for potential biases such as noon-
564 time fluorescence quenching and flexible chlorophyll-to-carbon fixation ratios ([Schuback et al.,](#)
565 [2018](#)). The broader suite of potential corrections as suggested by [Boatman et al. \(2019\)](#) and
566 [Schuback et al. \(2018\)](#) were not available to us during this study. The FRRF data were
567 subsequently compared to the NCP O₂/Ar data from which GPP rates were calculated. As the
568 NCP approach is based on changes of O₂ concentration in the water column, a photosynthetic
569 quotient (PQ; oxygen evolved to carbon fixed) was applied to convert rates into carbon units.
570 Generally, a PQ of 1.4 for NO₃⁻ supported production and 1.1 for NH₄⁺ supported production is
571 used. However, for simplicity and as the PQ can also vary with light induced stress ([Iriarte,](#)
572 [1999](#)) as well as other stress factors ([Spilling et al., 2015](#)), we used a PQ of 1.2 for all samples.
573 Changes in O₂/Ar include all photoautotrophic and heterotrophic activity. Hence, a positive trend
574 during the day indicates that photoautotrophy outweighs all chemoheterotrophy, including
575 phytoplankton respiratory processes. Daytime production includes all respiratory processes and
576 photosynthesis while nighttime data measures only respiratory processes. In order to estimate

577 GPP from diel cycles in O₂/Ar, we assume that the nighttime and daytime respiration rates are
578 equal.

579 Since no FRRF measurements were conducted during the P1604 cruise, GPP rates were only
580 obtained using the O₂/Ar data. The diurnal rate estimates followed distinct diurnal cycles with a
581 maximum production of around 160 mmol C m⁻² d⁻¹ and a daily average around 40 mmol C m⁻²
582 d⁻¹. As noted by ([Landry et al., 2011a](#)), carbon-based phytoplankton production measured from
583 dilution experiments exceed those from NPP_{14C} because they separately account for
584 phytoplankton biomass growth and production grazed by microzooplankton over the course of
585 24-h incubations while NPP_{14C} incorporates respiration losses of grazed ¹⁴C-labelled carbon into
586 the measurement. Hence, the difference in portions of GPP recovered by NPP_{14C} and NPP_{G/G}
587 might be interpreted as measure of production losses during transfer of the organic matter
588 through the food-web. P1706-C1 and C2 gave high GPP rates for both O₂/Ar and FRRF, with
589 daily mid-day maxima >3000 mmol C m⁻² d⁻¹ for C1 and >1000 mmol C m⁻² d⁻¹ C2. Direct
590 comparison of cycle means indicate that rates were not statistically significantly different
591 between methods ($p \geq 0.4$, t-test, Mann-Whitney Rank Sum test). GPP_{O₂/Ar} for P1706-C3 and C4
592 were compromised by the ship passing through different water masses frequently, which
593 precluded calculating day and night rates for the same water parcel. GPP rates were nonetheless
594 obtained for those cycles from FRRF data. Comparing NPP_{14C} and GPP_{FRRF} estimates for all
595 cycles showed a reasonable % of carbon loss: 36, 51, 27 and 40 of GPP for P1706-C1-C4,
596 respectively. For the CCE region, ~20% of fixed carbon is released to the DOC pool, with a
597 range between 7 and 44% (Goericke unpublished data; ([Stukel et al., 2012](#))). Respiration alone
598 can also reduce NPP on average by 9 to 22% ([López-Sandoval et al., 2014](#)). Higher as well as
599 lower ratios of NPP:GPP have been reported in literature (e.g. [Bercel & Kranz, 2019](#); [Kranz et](#)
600 [al., 2010](#)). In addition, measured O₂-based GPP estimates that are >200% of simultaneous NPP
601 measurements have been reported in field studies ([Hashimoto et al., 2005](#); [Laws et al., 2000](#)).
602 Hence our NPP/GPP ratios fall within expected ranges.

603 Some uncertainties of the GPP_{FRRF} merit discussion. The GPP_{FRRF} analysis is based on
604 daytime P vs. E curves, but estimates of the photosystem reaction centers (RCII) come from
605 nighttime sampling. Since the number of functional RCII varies throughout the day, over or
606 under estimates of rates may occur. In addition, our calculated GPP rates for the photic zone
607 come solely from phytoplankton sampled at 5-10 m depth. Despite dark or low-light acclimation

prior to measurements, the photosystem might not have had time to re-oxidize fully, resulting in underestimates of quantum yield and photochemical production. Moreover, surface communities might express different values in photosynthetic efficiency under low light intensities (α) and maximum photosynthetic rates compared to deep samples. This bias is apparent when analyzing the relatively fast diel changes (Fig. S1), which are likely faster than cell mixing in the water column. Hence, if deeper cells are better adapted to low-light conditions, calculated rates from the mixed layer might be underestimated. Nonetheless, since the MLD was relatively shallow for most cycles, we expect a relatively good estimate. Part of the temporal and spatial mismatch between GPP_{FRRF} and GPP_{EIMS} might also be explained by likely changes in the electron to C ratios occurring throughout the day which could partially decouple O₂ production from C-fixation. Lastly, due to the lack of pigment data, no spectral correction could be applied to our rate estimates ([Schuback et al., 2018](#)). Despite these shortcomings, the good agreement between FRRF and O₂/Ar methods gives us some confidence that both approaches can reliably estimate water-column GPP.

As changes in production are associated with the ability of phytoplankton to efficiently utilize light or dissipate excess light, photophysiological parameters as presented in (Fig. S1) can add a more mechanistic understanding of some of the presented production rates. A significant change in photophysiological responses was seen in the data for P1706-C2. The observed drop in maximum quantum yield (F_v/F_m) indicates conditions that negatively affect photosystem function in the phytoplankton community, such as iron (Fe) limitation. Iron limitation is not only associated with a loss in quantum yield efficiency but more importantly the optical absorption cross section of the photosystem (σ), the area of chlorophyll pigments available to absorb light around a reaction center, and the reoxidation rate of the Quinone A in PSII (1/ τ) ([Kolber et al., 1994](#)). Compared to P1706-C1, 1/ τ increased in our C2 measurements. This response was not expected as rates of electron transport usually decrease under Fe-limitation. However, Fe limitation during P1706-C2, was independently determined based on diagnostic nutrient ratios (Si:N and Fe:N; K. Fulton and K. Barbeau, pers. comm.) and Fe amendment experiments (K. Forsch and K. Barbeau, pers. comm.). Consequently, 1/ τ was likely driven by changes in the phytoplankton community. The enhanced NPQ rates (Fig S2) demonstrated an enhanced energy dissipation through non-photochemical processes in Fe limited communities. This enhanced NPQ_{NSV} did affect our productivity rate estimate, as NPQ_{NSV} values are used to calculate the

639 electron to carbon ratio (see Eq. 7; Schuback et al., 2018). Data on photophysiology will not be
640 discussed further, yet we decided to include those data here and in the supplemental material as
641 those datasets can inform the reader on underlying processes of productivity changes and
642 limitations thereof.

643 **5.2. Net community, New Production and Export Flux**

644 Nitrate consumed by phytoplankton often represents new production in the surface ocean and
645 hence should equate to the amount of organic matter available for export (Eppley & Peterson,
646 1979), although it may be an overestimate if substantial nitrification occurs within the euphotic
647 zone (Yool et al., 2007). Similarly, NCP represents the balance between organic matter
648 production (photosynthesis) and organic matter consumption (respiration); hence, should also
649 approximate export when the organic pools are at steady-state (Hamme et al., 2012; Li & Cassar,
650 2017). Crucially, we only expect a quantitative correspondence between NP, NCP and export
651 when integrating over sufficiently long temporal and large spatial scales (Plattner et al., 2005)
652 and including all forms of exported organic matter (Boyd et al., 2019; Ducklow et al., 2001).
653 Thus comparisons of these kinds of measurements for short term in-situ or shipboard incubations
654 in spatially heterogeneous regions like the CCE can be challenging to interpret.

655 Until recently O₂:Ar-based NCP estimates were only used in near-steady-state systems,
656 assuming that timeframes for NCP measurements (weeks to months) need to integrate all past
657 changes in production, grazing and physical disturbances. More recently, Teeter et al. (2018)
658 showed that a strict steady-state assumption for NCP analysis is not required and that reliable
659 rates of NCP can be obtained even if the community varies. This is because the NCP estimate is
660 a weighted analysis of the current oxygen inventory combined with prior gas fluxes for which
661 most weight is placed on the recent past. The weighting reduces historical influence and
662 enhances more recent events. However, the uncertainty of the NCP estimate increases with the
663 physical complexity of a region (Teeter et al., 2018). Due to the complex physical and
664 biochemical nature of the CCE ecosystem, large discrepancies were expected in our method
665 comparison. For example, although upwelling is typically associated with high primary
666 production, the low oxygen content of freshly upwelled waters could be interpreted as negative
667 NCP. On the other hand, upwelled water with accumulated biomass and high oxygen from the
668 primary production would appear to be strongly net autotrophic, even if NCP had switched to

negative. Despite these potential issues, the EIMS method has been usefully applied in other complex coastal environments, such as the Western Antarctic Peninsula ([Eveleth et al., 2017](#); [Tortell et al., 2014](#)). Since we applied the EIMS method with a Lagrangian study, we are also able to measure changes in the O₂/Ar ratio with high temporal resolution and resolve some of the uncertainties in measured signal vs. true activity ([Teeter et al., 2018](#); [Wang et al., submitted](#)).

Using the calculation of NCP_{inst}, NCP production estimates should match the combined effects of NP and short-term changes in organic matter inventories. Our direct comparison reveals large mismatches, however (Fig 5, Table 1, S4). Four factors play an important role here: 1) NP estimates can never be negative while NCP can be negative, especially in a high-biomass system when grazing exceeds production over the timeframe of measurements; 2) vertical advection or diffusion across isopycnals can introduce low oxygen water into surface layers; 3) NCP rates are influenced by all organisms in the mixed layer, some of which undergo diurnal vertical migration and therefore introduce a vertical transport component to the mass balance; and 4) our Lagrangian approach was partially affected by ship movements during net tows and instrument recovery which introduce a non-lagrangian error into NCP measurements.

As presented in Results, our data show substantial discrepancies between NCP and NP. During P1604-C2 and C4, when regions of high variability were intentionally avoided, there was reasonable agreement, despite statistical differences, between NCP_{RT} and NP measurements (NCP_{inst} = 6.0 ± 0.1 and NP = 10.6 ± 2.7 mmol C m⁻² d⁻¹ for P1604-C2; NCP_{inst} = 16.4 ± 4.0 and NP = 23.2 ± 5.9 mmol C m⁻² d⁻¹ for P1604-C4). For P1604-C3, however, NP was relatively high and positive (23.8 ± 8 mmol C m⁻² d⁻¹) while NCP_{inst} was negative (-0.1 ± 1.1 mmol C m⁻² d⁻¹). On this cycle, surface Chl (1.0 µg L⁻¹), surface NO₃⁻ (3.8 µmol L⁻¹) and surface POC (7.1 µmol C L⁻¹) were all high, but a dense swarm of doliolids, with high grazing and presumably high respiration, dominated the zooplankton ([Morrow et al., 2018](#)). It is thus likely that the discrepancy in P1604-C3 measurements was due to circumstances in which NCP and NP were temporarily decoupled, with nitrate fueling substantial NP even as high mesozooplankton grazing and respiration drove NCP towards net heterotrophy.

For P1706, the differences between NCP and NP were more pronounced. NP was reasonably high on all cycles, with mean *f*-ratios varying from 0.27 to 0.49. NCP_{inst} was high on P1706-C1 (although still only 49% of NP), but negative or near zero on all other cycles. These results might

be explained by the unusual physical and biological dynamics of the mesoscale filament that was studied on this cruise. Specifically, the cruise targeted non-steady-state water parcels ranging from coastal upwelling on C1 to aged filament water mixed with offshore California Current water on C3, as well as water parcels during early and late stages of a filament evolution (P1706-C2 and C4). Along this continuum from upwelling to offshore mixing, surface POC declined substantially from 38.5 to 5.7 $\mu\text{mol C L}^{-1}$ for P1706-C1 to C4. This biomass decline (during offshore transit over 2-3 weeks) would have to be matched by a combination of export and/or negative NCP along the transect. However, NP cannot be negative, and although NO_3^- decreased from inshore to offshore, surface nitrate remained relatively high ($2.9 \mu\text{mol C L}^{-1}$) allowing continued new production. Ammonium also accumulated between P1706-C1 and P1706-C4 (from 0.4 to 1.8 $\mu\text{mol L}^{-1}$), as would be expected if remineralization exceeded phytoplankton production. Our results are thus consistent with a system in which NCP peaked early in the bloom and switched to negative as the bloom declined. A similar NP and NCP pattern was observed following a coastal Antarctic bloom ([Stukel et al., 2015b](#); [Tortell et al., 2014](#)). The NCP estimates could also have been affected by upwelling and/or vertical diffusion in this energetic mesoscale environment, which would underestimate NCP if low O_2 water was introduced from below the mixed layer ([Wang et al. \(submitted\)](#) for potential impact on NCP). In addition, nitrate uptake could overestimate NP if substantial nitrification occurs in the euphotic zone. This would seem an unlikely scenario, given estimates of mixed-layer nitrification in the CCE ($4.6 \text{ nmol L}^{-1} \text{ d}^{-1}$; [Santoro et al., 2013](#)) that are relatively low compared to nitrate uptake rates. However, nitrification might be more active in filaments.

Ultimately, NP and NCP should be balanced by export production. Our results show, however, that export flux was substantially lower than NP across the region (Fig. 5). When integrated to the base of the euphotic zone (data not shown) to match sediment trap data, NP exceeded export for all three cycles of P1604 and for all cycles of P1706 except C4 (at the end of the filament). For all the cycles of P1706, NP averaged 2.7 times higher than sinking flux. The same pattern did not hold for NCP in P1706 because of multiple cycles with negative NCP. In a non-steady state system, however, export should be balanced not by NCP alone, but by the sum of NCP and POC decline, unless large parts of NCP are also going into DOC buildup. Because P1706-C4 was a transport extension of C2, we can test this balance over the 12 days that separate the beginning and end of those cycles. Over this period, POC declined from 1078 to 510 mmol C

730 m^{-2} , equating to a decline of $43.6 \text{ mmol C m}^{-2} \text{ d}^{-1}$. This is remarkably equal to the mean export
731 during these two cycles ($40.1 \text{ mmol C m}^{-2} \text{ d}^{-1}$), suggesting that the declining biomass would have
732 been sufficient to support all the measured export flux even if no additional biomass was
733 produced.

734 The measurement of new production in excess of sinking flux is not a novel result. Nitrate
735 uptake has also been reported to exceed the sinking particle export in the Western Antarctic
736 Peninsula (Ducklow et al., 2018; Stukel et al., 2015a), the Bermuda Atlantic Time-Series site
737 (Lipschultz, 2001; Lomas et al., 2013), the Arabian Sea (Buesseler et al., 1998; Sambrotto,
738 2001), and the Costa Rica Dome (Stukel et al., 2016). In addition, NCP has been found to exceed
739 sinking flux in the Sargasso Sea (Estapa et al., 2015) and the Western Antarctic Peninsula
740 (Stukel et al., 2015a). Within the CCE, prior studies have determined e-ratios of ~ 0.2 (Kelly et
741 al., 2018), compared to f-ratios frequently > 0.5 (Harrison et al., 1987) and a region-wide
742 NCP/NPP ratio of 0.4 (Munro et al., 2013). This deficiency of sinking export relative to NP and
743 NCP likely reflects the importance of non-sinking forms of export including active transport of
744 carbon by diel vertical migrants (Bianchi et al., 2013; Steinberg et al., 2000) and subduction of
745 particulate and dissolved organic matter (Carlson et al., 1994; Omand et al., 2015). Within the
746 CCE, subduction of particles has been shown to be a substantial flux of organic matter out of the
747 euphotic zone, although subducted particles did not penetrate deep into the ocean interior (Stukel
748 et al., 2018). Active transport has also been shown to be substantial, and even to rival sinking
749 flux, in high biomass regions of the CCE (Kelly et al., 2019). Together, these other processes
750 likely explain our measurement discrepancies between NP and export.

751 6. Conclusions

752 Our study presents a well-constrained characterization of gross primary production, net
753 primary production, net community production, new production, and export production in a
754 complex and heterogeneous physical environment. The results show how a multi-method
755 approach can clarify some of the variabilities and inconsistencies observed using different
756 methods. We found strong spatial gradients in productivity rates from coastal to offshore regions
757 that were primarily driven by decreasing biomass and nutrient availability with distance from
758 shore, and we showed that the high-resolution measurements applied here resolved diel patterns
759 in GPP and NCP. Overall, all our data from temporally resolved production estimates are

760 surprisingly consistent, within the errors of the estimates, with data from traditional 24-h
761 production measurements. The GPP:NPP ratio was approximately 2 over the study region, with
762 no distinct spatial pattern. The *f*-ratios (NP:NPP) varied from 0.16 to 0.55, suggesting that
763 recycled NH₄⁺ was typically the most important nutrient supporting production, even though
764 nitrate was still a major source of N. New production typically exceeded carbon export of
765 sinking particles by a large margin, suggesting that temporally and spatially decoupled export
766 (vertical migration of grazers, water mass subduction) must be quantitatively important for
767 resolving the region's carbon budget. Since underway high temporal resolution analyses of
768 productivity using FRRF and EIMS match general ecosystem expectations, we suggest that
769 temporally resolved production methods should be employed regularly to enhance understanding
770 of physically complex and economically important ecosystems.

771

772 **7. Acknowledgements, Samples and Data:**

773 The authors declare no conflict of interest. Data reported and presented in this study can be
774 accessed at the CCE-LTER Datazoo online database (archiving is underway during the
775 manuscript review process).

776 This study was funded by US National Science Foundation grants OCE-1637632 (CCE-
777 LTER) and -1614359 (RAPID). We appreciate the contributions to shipboard sampling and
778 analyses by Ali Freibott, Belli Valencia, Shonna Dovel and Megan Roadman and Cameron
779 Quackenbush. We also want to thank the captains and the crews of the *R/V Sikuliaq* and *R/V*
780 *Roger Revelle* for their support. We appreciated the help during both cruises by Chief scientist
781 Mark Ohman. We also want to thank Kathy Barbeau and Kiefer Forsch for their discussion of
782 their preliminary data on iron limitation during these cruises.

783

784 **References**

- 785
- 786 Barron, R. K., Siegel, D. A., & Guillocheau, N. (2014). Evaluating the importance of
787 phytoplankton community structure to the optical properties of the Santa Barbara
788 Channel, California. *Limnology and Oceanography*, 59(3), 927-946.
- 789 Behrenfeld, M. J., & Falkowski, P. G. (1997). Photosynthetic rates derived from satellite-based
790 chlorophyll concentration. *Limnology and Oceanography*, 42(1), 1-20.
- 791 Bercel, T. L., & Kranz, S. A. (2019). Insights into carbon acquisition and photosynthesis in
792 Karenia brevis under a range of CO₂ concentrations. *Progress in Oceanography*, 172,
793 65-76.
- 794 Bianchi, D., Stock, C., Galbraith, E. D., & Sarmiento, J. L. (2013). Diel vertical migration:
795 Ecological controls and impacts on the biological pump in a one-dimensional ocean
796 model. *Global Biogeochemical Cycles*, 27(2), 478-491.
- 797 Boatman, T. G., Geider, R. J., & Oxborough, K. (2019). Improving the accuracy of single
798 turnover active fluorometry (STAF) for the estimation of phytoplankton primary
799 productivity (PhytoPP). *bioRxiv*, 583591.
- 800 Bond, N. A., Cronin, M. F., Freeland, H., & Mantua, N. (2015). Causes and impacts of the 2014
801 warm anomaly in the NE Pacific. *Geophysical Research Letters*, 42(9), 3414-3420.
- 802 Boyd, P. W., Claustre, H., Levy, M., Siegel, D. A., & Weber, T. (2019). Multi-faceted particle
803 pumps drive carbon sequestration in the ocean. *Nature*, 568(7752), 327-335.
- 804 Bronk, D. A., Glibert, P. M., & Ward, B. B. (1994). Nitrogen uptake, dissolved organic nitrogen
805 release, and new production. *Science*, 265(5180), 1843-1846.
- 806 Buesseler, K., Ball, L., Andrews, J., Benitez-Nelson, C., Belastock, R., Chai, F., & Chao, Y.
807 (1998). Upper ocean export of particulate organic carbon in the Arabian Sea derived from
808 thorium-234. *Deep-Sea Research II*, 45(10-11), 2461-2487.

- 809 Carlson, C. A., Ducklow, H. W., & Michaels, A. F. (1994). Annual Flux of Dissolved Organic-
810 Carbon from the Euphotic Zone in the Northwestern Sargasso Sea. *Nature*, 371(6496),
811 405-408.
- 812 Cassar, N., Barnett, B. A., Bender, M. L., Kaiser, J., Hamme, R. C., & Tilbrook, B. (2009).
813 Continuous high-frequency dissolved O₂/Ar measurements by equilibrator inlet mass
814 spectrometry. *Analytical Chemistry*, 81(5), 1855-1864.
- 815 Chavez, F. P., & Messie, M. (2009). A comparison of Eastern Boundary Upwelling Ecosystems.
816 *Progress in Oceanography*, 83(1-4), 80-96.
- 817 Collos, Y. (1998). Nitrate uptake, nitrite release and uptake, and new production estimates.
818 *Marine Ecology Progress Series*, 171, 293-301.
- 819 Ducklow, H. W., Steinberg, D. K., & Buesseler, K. O. (2001). Upper ocean carbon export and
820 the biological pump. *Oceanography* 14(4), 0-58.
- 821 Ducklow, H. W., Stukel, M. R., Eveleth, R., Doney, S. C., Jickells, T., Schofield, O., et al.
822 (2018). Spring-summer net community production, new production, particle export and
823 related water column biogeochemical processes in the marginal sea ice zone of the
824 Western Antarctic Peninsula 2012-2014. *Philosophical Transactions of the Royal Society
a-Mathematical Physical and Engineering Sciences*, 376(2122).
- 826 Dugdale, R. C. (1972). Chemical oceanography and primary productivity in upwelling regions.
827 *Geoforum*, 3(3), 47-61.
- 828 Dugdale, R. C., & Goering, J. J. (1967). Uptake of New and Regenerated Forms of Nitrogen in
829 Primary Productivity. *Limnology and Oceanography*, 12(2), 196-206.
- 830 Dugdale, R. C., & Wilkerson, F. P. (1986). The Use of ¹⁵N to Measure Nitrogen Uptake in
831 Eutrophic Oceans - Experimental Considerations. *Limnology and Oceanography*, 31(4),
832 673-689.

- 833 Dunne, J. P., Sarmiento, J. L., & Gnanadesikan, A. (2007). A synthesis of global particle export
834 from the surface ocean and cycling through the ocean interior and on the seafloor. *Global*
835 *Biogeochemical Cycles*, 21(4).
- 836 Eppley, R. W., & Peterson, B. J. (1979). Particulate Organic-Matter Flux and Planktonic New
837 Production in the Deep Ocean. *Nature*, 282(5740), 677-680.
- 838 Estapa, M. L., Siegel, D. A., Buesseler, K. O., Stanley, R. H. R., Lomas, M. W., & Nelson, N. B.
839 (2015). Decoupling of net community and export production on submesoscales. *Global*
840 *Biogeochemical Cycles*, 29(8), 1266-1282.
- 841 Eveleth, R., Cassar, N., Doney, S. C., Munro, D. R., & Sweeney, C. (2017). Biological and
842 physical controls on O₂/Ar, Ar and pCO₂ variability at the Western Antarctic Peninsula
843 and in the Drake Passage. *Deep Sea Research II*, 139, 77-88.
- 844 Falkowski, P. G., & Kolber, Z. (1993). *Estimation of Phytoplankton Photosynthesis by Active*
845 *Fluorescence*. Paper presented at the Measurement of Primary Production from the
846 Molecular to the Global Scale.
- 847 Goldman, J. A. L., Kranz, S. A., Young, J. N., Tortell, P. D., Stanley, R. H. R., Bender, M. L., &
848 Morel, F. M. M. (2015). Gross and net production during the spring bloom along the
849 Western Antarctic Peninsula. *New Phytologist*, 205(1), 182-191.
- 850 Gordon, L. I., Jennings, J. C., Ross, A. A., & Krest, J. M. (1992). A suggested Protocol for
851 Continuous Flow Automated Analysis of Seawater Nutrients in the WOCE Hydrographic
852 Program and the Joint Global Ocean Fluxes Study Grp. *Tech Rpt OSU College of*
853 *Oceanography Descr. Chem Oc.*, 92(1).
- 854 Hamme, R. C., Cassar, N., Lance, V. P., Vaillancourt, R. D., Bender, M. L., Strutton, P. G., et al.
855 (2012). Dissolved O₂/Ar and other methods reveal rapid changes in productivity during a
856 Lagrangian experiment in the Southern Ocean. *Journal of Geophysical Research-Oceans*,
857 117(C4).
- 858 Harrison, W. G., Platt, T., & Lewis, M. R. (1987). F-Ratio and Its Relationship to Ambient
859 Nitrate Concentration in Coastal Waters. *Journal of Plankton Research*, 9(1), 235-248.

- 860 Hashimoto, S., Horimoto, N., Yamaguchi, Y., Ishimaru, T., & Saino, T. (2005). Relationship
861 between net and gross primary production in the Sagami Bay, Japan. *Limnology and*
862 *Oceanography*, 50(6), 1830-1835.
- 863 Iriarte, A. (1999). The influence of irradiance on the apparent photosynthetic quotient in the
864 unicellular alga *Pycnococcus provasolii*. *Cahiers De Biologie Marine*, 40(1), 29-33.
- 865 Jacox, M. G., Hazen, E. L., Zaba, K. D., Rudnick, D. L., Edwards, C. A., Moore, A. M., &
866 Bograd, S. J. (2016). Impacts of the 2015-2016 El Nino on the California Current
867 System: Early assessment and comparison to past events. *Geophysical Research Letters*,
868 43(13), 7072-7080.
- 869 Kahru, M., Jacox, M. G., Lee, Z., Kudela, R. M., Manzano-Sarabia, M., & Mitchell, B. G.
870 (2015). Optimized multi-satellite merger of primary production estimates in the
871 California Current using inherent optical properties. *Journal of Marine Systems*, 147, 94-
872 102.
- 873 Kanda, J., Itoh, T., Ishikawa, D., & Watanabe, Y. (2003). Environmental control of nitrate
874 uptake in the East China Sea. *Deep-Sea Research II*, 50(2), 403-422.
- 875 Kelly, T. B., Davison, P. C., Goericke, R., Landry, M. R., Ohman, M. D., & Stukel, M. R.
876 (2019). The Importance of Mesozooplankton Diel Vertical Migration for Sustaining a
877 Mesopelagic Food Web. *bioRxiv*, 642975.
- 878 Kelly, T. B., Goericke, R., Kahru, M., Song, H., & Stukel, M. R. (2018). CCE II: Spatial and
879 interannual variability in export efficiency and the biological pump in an eastern
880 boundary current upwelling system with substantial lateral advection. *Deep-Sea Research*
881 *I* 140, 14-25.
- 882 Knauer, G. A., Martin, J. H., & Bruland, K. W. (1979). Fluxes of Particulate Carbon, Nitrogen,
883 and Phosphorus in the Upper Water Column of the Northeast Pacific. *Deep-Sea Research*
884 *I* 26(1), 97-108.
- 885 Kolber, Z., & Falkowski, P. G. (1993). Use of Active Fluorescence to Estimate Phytoplankton
886 Photosynthesis in-Situ. *Limnology and Oceanography*, 38(8), 1646-1665.

- 887 Kolber, Z. S., Barber, R. T., Coale, K. H., Fitzwater, S. E., Greene, R. M., Johnson, K. S., et al.
888 (1994). Iron Limitation of Phytoplankton Photosynthesis in the Equatorial Pacific-Ocean.
889 *Nature*, 371(6493), 145-149.
- 890 Kranz, S. A., Levitan, O., Richter, K.-U., Prasil, O., Berman-Frank, I., & Rost, B. (2010).
891 Combined effects of CO₂ and light on the N₂-fixing cyanobacterium *Trichodesmium*
892 IMS101: Physiological responses. *Plant Physiology* 154(1), 334-345.
- 893 Kudela, R. M., Banas, N. S., Barth, J. A., Frame, E. R., Jay, D. A., Largier, J. L., et al. (2008).
894 New Insights into the Controls and Mechanisms of Plankton Productivity in Coastal
895 Upwelling Waters of the Northern California Current System. *Oceanography*, 21(4), 46-
896 59.
- 897 Kumar, N., Anderson, R. F., Mortlock, R. A., Froelich, P. N., Kubik, P., Dittrichhannen, B., &
898 Suter, M. (1995). Increased Biological Productivity and Export Production in the Glacial
899 Southern-Ocean. *Nature*, 378(6558), 675-680.
- 900 Landry, M. R., Brown, S. L., Rii, Y. M., Selph, K. E., Bidigare, R. R., Yang, E. J., & Simmons,
901 M. P. (2008). Depth-stratified phytoplankton dynamics in Cyclone Opal, a subtropical
902 mesoscale eddy. *Deep-Sea Research II*, 55(10-13), 1348-1359.
- 903 Landry, M. R., Constantinou, J., Latasa, M., Brown, S. L., Bidigare, R. R., & Ondrusek, M. E.
904 (2000). Biological response to iron fertilization in the eastern equatorial Pacific (IronEx
905 II). III. Dynamics of phytoplankton growth and microzooplankton grazing. *Marine
906 Ecology Progress Series*, 201, 57-72.
- 907 Landry, M. R., & Hassett, R. P. (1982). Estimating the Grazing Impact of Marine Micro-
908 Zooplankton. *Marine Biology*, 67(3), 283-288.
- 909 Landry, M. R., Ohman, M. D., Goericke, R., Stukel, M. R., Barbeau, K. A., Bundy, R., & Kahru,
910 M. (2012). Pelagic community responses to a deep-water front in the California Current
911 Ecosystem: overview of the A-Front Study. *Journal of Plankton Research*, 34(9), 739-
912 748.

- 913 Landry, M. R., Selph, K. E., Decima, M., Gutierrez-Rodriguez, A., Stukel, M. R., Taylor, A. G.,
914 & Pasulka, A. L. (2016). Phytoplankton production and grazing balances in the Costa
915 Rica Dome. *Journal of Plankton Research*, 38(2), 366-379.
- 916 Landry, M. R., Selph, K. E., Taylor, A. G., Decima, M., Balch, W. M., & Bidigare, R. R.
917 (2011a). Phytoplankton growth, grazing and production balances in the HNLC equatorial
918 Pacific. *Deep-Sea Research II*, 58(3-4), 524-535.
- 919 Landry, M. R., Selph, K. E., & Yang, E. J. (2011b). Decoupled phytoplankton growth and
920 microzooplankton grazing in the deep euphotic zone of the eastern equatorial Pacific.
921 *Marine Ecology Progress Series*, 421, 13-24.
- 922 Lawrenz, E., Silsbe, G., Capuzzo, E., Ylostalo, P., Forster, R. M., Simis, S. G. H., et al. (2013).
923 Predicting the Electron Requirement for Carbon Fixation in Seas and Oceans. *PLoS ONE*,
924 8(3).
- 925 Laws, E. A., Landry, M. R., Barber, R. T., Campbell, L., Dickson, M. L., & Marra, J. (2000).
926 Carbon cycling in primary production bottle incubations: inferences from grazing
927 experiments and photosynthetic studies using (14)C and (18)O in the Arabian Sea. *Deep-*
928 *Sea Research II*, 47(7-8), 1339-1352.
- 929 Li, Q. P., Franks, P. J. S., Landry, M. R., Goericke, R., & Taylor, A. G. (2010). Modeling
930 phytoplankton growth rates and chlorophyll to carbon ratios in California coastal and
931 pelagic ecosystems. *Journal of Geophysical Research-Biogeosciences*, 115.
- 932 Li, Z. C., & Cassar, N. (2017). A mechanistic model of an upper bound on oceanic carbon export
933 as a function of mixed layer depth and temperature. *Biogeosciences*, 14(22), 5015-5027.
- 934 Lipschultz, F. (2001). A time-series assessment of the nitrogen cycle at BATS. *Deep-Sea*
935 *Research II*, 48(8-9), 1897-1924.
- 936 Lomas, M. W., Bates, N. R., Johnson, R. J., Knap, A. H., Steinberg, D. K., & Carlson, C. A.
937 (2013). Two decades and counting: 24-years of sustained open ocean biogeochemical
938 measurements in the Sargasso Sea. *Deep-Sea Research II*, 93, 16-32.

- 939 Longhurst, A., Sathyendranath, S., Platt, T., & Caverhill, C. (1995). An Estimate of Global
940 Primary Production in the Ocean from Satellite Radiometer Data. *Journal of Plankton*
941 *Research*, 17(6), 1245-1271.
- 942 López-Sandoval, D. C., Rodríguez-Ramos, T., Cermeño, P., Sobrino, C., & Marañón, E. (2014).
943 Photosynthesis and respiration in marine phytoplankton: Relationship with cell size,
944 taxonomic affiliation, and growth phase. *Journal of Experimental Marine Biology and*
945 *Ecology*, 457, 151-159.
- 946 Luz, B., & Barkan, E. (2005). The isotopic ratios $^{17}\text{O}/^{16}\text{O}$ and $^{18}\text{O}/^{16}\text{O}$ in molecular oxygen and
947 their significance in biogeochemistry. *Geochimica et Cosmochimica Acta*, 69(5), 1099-
948 1110.
- 949 Marra, J. (2009). Net and gross productivity: Weighing in with ^{14}C . *Aquatic Microbial Ecology*
950 56(2), 123-131
951 .
- 952 Michaels, A. F., & Silver, M. W. (1988). Primary Production, Sinking Fluxes and the Microbial
953 Food Web. *Deep-Sea Research I* 35(4), 473-490.
- 954 Moore, C. M., Suggett, D. J., Hickman, A. E., Kim, Y. N., Tweddle, J. F., Sharples, J., et al.
955 (2006). Phytoplankton photoacclimation and photoadaptation in response to
956 environmental gradients in a shelf sea. *Limnology and Oceanography*, 51(2), 936-949.
- 957 Morrow, R. M., Ohman, M. D., Goericke, R., Kelly, T. B., Stephens, B. M., & Stukel, M. R.
958 (2018). CCE V: Primary production, mesozooplankton grazing, and the biological pump
959 in the California Current Ecosystem: Variability and response to El Niño. *Deep-Sea*
960 *Research I* 140, 52-62.
- 961 Muller-Karger, F. E., Varela, R., Thunell, R., Luerssen, R., Hu, C. M., & Walsh, J. J. (2005). The
962 importance of continental margins in the global carbon cycle. *Geophysical Research*
963 *Letters*, 32(1).

- 964 Munro, D. R., Quay, P. D., Juranek, L. W., & Goericke, R. (2013). Biological production rates
965 off the Southern California coast estimated from triple O₂ isotopes and O₂ : Ar gas ratios.
966 *Limnology and Oceanography*, 58(4), 1312-1328.
- 967 Myklestad, S. M. (2000). *The Handbook of Environmental Chemistry* (Vol. Vol. 5D): Springer.
- 968 Nagai, T., Gruber, N., Frenzel, H., Lachkar, Z., McWilliams, J. C., & Plattner, G. K. (2015).
969 Dominant role of eddies and filaments in the offshore transport of carbon and nutrients in
970 the California Current System. *Journal of Geophysical Research-Oceans*, 120(8), 5318-
971 5341.
- 972 Nickels, C. F., & Ohman, M. D. (2018). CCEIII: Persistent functional relationships between
973 copepod egg production rates and food concentration through anomalously warm
974 conditions in the California Current Ecosystem. *Deep-Sea Research I* 140, 26-35.
- 975 O'Reilly, J. E., Maritorena, S., Mitchell, B. G., Siegel, D. A., Carder, K. L., Garver, S. A., et al.
976 (1998). Ocean color chlorophyll algorithms for SeaWiFS. *Journal of Geophysical
977 Research-Oceans*, 103(C11), 24937-24953.
- 978 Ohman, M. D., Powell, J. R., Picheral, M., & Jensen, D. W. (2012). Mesozooplankton and
979 particulate matter responses to a deep-water frontal system in the southern California
980 Current System. *Journal of Plankton Research*, 34(9), 815-827.
- 981 Omand, M. M., D'Asaro, E. A., Lee, C. M., Perry, M. J., Briggs, N., Cetinic, I., & Mahadevan,
982 A. (2015). Eddy-driven subduction exports particulate organic carbon from the spring
983 bloom. *Science*, 348(6231), 222-225.
- 984 Oxborough, K., Moore, C. M., Suggett, D. J., Lawson, T., Chan, H. G., & Geider, R. J. (2012).
985 Direct estimation of functional PSII reaction center concentration and PSII electron flux
986 on a volume basis: a new approach to the analysis of Fast Repetition Rate fluorometry
987 (FRRf) data. *Limnology and Oceanography-Methods*, 10, 142-154.
- 988 Painter, S. C., Sanders, R., Poulton, A. J., Woodward, E. M. S., Lucas, M., & Chamberlain, K.
989 (2007). Nitrate uptake at photic zone depths is not important for export in the subtropical
990 ocean. *Global Biogeochemical Cycles*, 21(4).

- 991 Pan, X. J., Mannino, A., Marshall, H. G., Filippino, K. C., & Mulholland, M. R. (2011). Remote
992 sensing of phytoplankton community composition along the northeast coast of the United
993 States. *Remote Sensing of Environment*, 115(12), 3731-3747.
- 994 Peterson, B. J. (1980). Aquatic Primary Productivity and the C₁₄-CO₂ Method - a History of the
995 Productivity Problem. *Annual Review of Ecology and Systematics*, 11, 359-385.
- 996 Platt, T., Gallegos, C. L., & Harrison, W. G. (1980). Photoinhibition of Photosynthesis in Natural
997 Assemblages of Marine-Phytoplankton. *Journal of Marine Research*, 38(4), 687-701.
- 998 Plattner, G. K., Gruber, N., Frenzel, H., & McWilliams, J. C. (2005). Decoupling marine export
999 production from new production. *Geophysical Research Letters*, 32(11).
- 1000 Quay, P. D., Peacock, C., Bjorkman, K., & Karl, D. M. (2010). Measuring primary production
1001 rates in the ocean: Enigmatic results between incubation and non-incubation methods at
1002 Station ALOHA. *Global Biogeochemical Cycles*, 24.
- 1003 Reuer, M. K., Barnett, B. A., Bender, M. L., Falkowski, P. G., & Hendricks, M. B. (2007). New
1004 estimates of Southern Ocean biological production rates from O-2/Ar ratios and the triple
1005 isotope composition of O-2. *Deep-Sea Research I* 54(6), 951-974.
- 1006 Robinson, C., Tilstone, G. H., Rees, A. P., Smyth, T. J., Fishwick, J. R., Tarran, G. A., et al.
1007 (2009). Comparison of in vitro and in situ plankton production determinations. *Aquatic
1008 Microbial Ecology*, 54(1), 13-34.
- 1009 Saba, V. S., Friedrichs, M. A. M., Antoine, D., Armstrong, R. A., Asanuma, I., Behrenfeld, M.
1010 J., et al. (2011). An evaluation of ocean color model estimates of marine primary
1011 productivity in coastal and pelagic regions across the globe. *Biogeosciences*, 8(2), 489-
1012 503.
- 1013 Sambrotto, R. N. (2001). Nitrogen production in the northern Arabian Sea during the Spring
1014 Intermonsoon and Southwest Monsoon seasons. *Deep-Sea Research II*, 48(6-7), 1173-
1015 1198.

- 1016 Santoro, A. E., Sakamoto, C. M., Smith, J. M., Plant, J. N., Gehman, A. L., Worden, A. Z., et al.
1017 (2013). Measurements of nitrite production in and around the primary nitrite maximum in
1018 the central California Current. *Biogeosciences*, 10(11), 7395-7410.
- 1019 Schuback, N., Hoppe, C. J. M., Tremblay, J. E., Maldonado, M. T., & Tortell, P. D. (2018).
1020 Primary productivity and the coupling of photosynthetic electron transport and carbon
1021 fixation in the Arctic Ocean (vol 62, pg 898, 2017). *Limnology and Oceanography*, 63(3),
1022 1444-1444.
- 1023 Schuback, N., & Tortell, P. D. (2019). Diurnal regulation of photosynthetic light absorption,
1024 electron transport and carbon fixation in two contrasting oceanic environments.
1025 *Biogeosciences*, 16(7), 1381-1399.
- 1026 Spilling, K., Ylostalo, P., Simis, S., & Seppala, J. (2015). Interaction Effects of Light,
1027 Temperature and Nutrient Limitations (N, P and Si) on Growth, Stoichiometry and
1028 Photosynthetic Parameters of the Cold-Water Diatom *Chaetoceros wighamii*. *PLoS ONE*,
1029 10(5).
- 1030 Steemann Nielsen, E. (1952). he Use of Radio-active Carbon (C14) for Measuring Organic
1031 Production in the Sea. *ICES Journal of Marine Science*, 18(2), 117-140.
- 1032 Steinberg, D. K., Carlson, C. A., Bates, N. R., Goldthwait, S. A., Madin, L. P., & Michaels, A. F.
1033 (2000). Zooplankton vertical migration and the active transport of dissolved organic and
1034 inorganic carbon in the Sargasso Sea. *Deep-Sea Research I* 47(1), 137-158.
- 1035 Stock, C., & Dunne, J. (2010). Controls on the ratio of mesozooplankton production to primary
1036 production in marine ecosystems. *Deep-Sea Research I*, 57(1), 95-112.
- 1037 Strickland, J. D., & Parsons, T. R. (1972). A practical handbook of seawater analysis, second ed.
1038 *Bulletin of the Fisheries Research Board of Canada*, 167.
- 1039 Stukel, M. R., Asher, E., Couto, N., Schofield, O., Strebel, S., Tortell, P., & Ducklow, H. W.
1040 (2015a). The imbalance of new and export production in the western Antarctic Peninsula,
1041 a potentially "leaky" ecosystem. *Global Biogeochemical Cycles*, 29(9), 1400-1420.

- 1042 Stukel, M. R., Benitez-Nelson, C. R., Decima, M., Taylor, A. G., Buchwald, C., & Landry, M. R.
1043 (2016). The biological pump in the Costa Rica Dome: an open-ocean upwelling system
1044 with high new production and low export. *Journal of Plankton Research*, 38(2), 348-365.
- 1045 Stukel, M. R., Goericke, R., & Landry, M. R. (2019a). Predicting primary production in the
1046 southern California Current Ecosystem from chlorophyll, nutrient concentrations, and
1047 irradiance. *bioRxiv*, 590240.
- 1048 Stukel, M. R., Kahru, M., Benitez-Nelson, C. R., Decima, M., Goericke, R., Landry, M. R., &
1049 Ohman, M. D. (2015b). Using Lagrangian-based process studies to test satellite
1050 algorithms of vertical carbon flux in the eastern North Pacific Ocean. *Journal of*
1051 *Geophysical Research-Oceans*, 120(11), 7208-7222.
- 1052 Stukel, M. R., Kelly, T. B., Aluwihare, L. I., Barbeau, K. A., Goericke, R., Krause, J. W., et al.
1053 (2019b). The Carbon:(234)Thorium ratios of sinking particles in the California current
1054 ecosystem 1: relationships with plankton ecosystem dynamics. *Marine chemistry*, 212, 1-
1055 15.
- 1056 Stukel, M. R., Landry, M. R., Ohman, M. D., Goericke, R., Samo, T., & Benitez-Nelson, C. R.
1057 (2012). Do inverse ecosystem models accurately reconstruct plankton trophic flows?
1058 Comparing two solution methods using field data from the California Current. *Journal of*
1059 *Marine Systems*, 91(1), 20-33.
- 1060 Stukel, M. R., Ohman, M. D., Benitez-Nelson, C. R., & Landry, M. R. (2013). Contributions of
1061 mesozooplankton to vertical carbon export in a coastal upwelling system. *Marine*
1062 *Ecology Progress Series*, 491, 47-+.
- 1063 Stukel, M. R., Song, H., Goericke, R., & Miller, A. J. (2018). The role of subduction and
1064 gravitational sinking in particle export, carbon sequestration, and the remineralization
1065 length scale in the California Current Ecosystem. *Limnology and Oceanography*, 63(1),
1066 363-383.

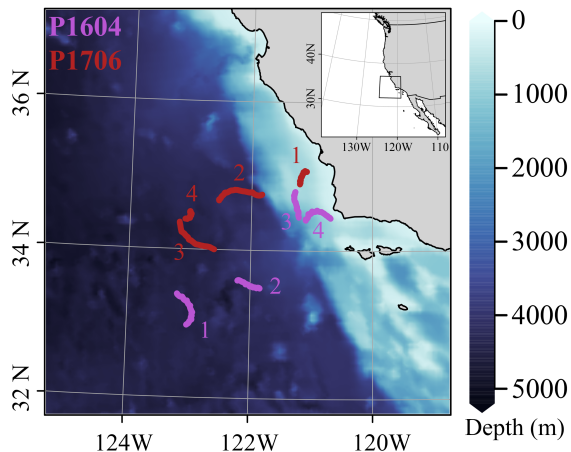
- 1067 Suggett, D., Kraay, G., Holligan, P., Davey, M., Aiken, J., & Geider, R. (2001). Assessment of
1068 photosynthesis in a spring cyanobacterial bloom by use of a fast repetition rate
1069 fluorometer. *Limnology and Oceanography*, 46(4), 802-810.
- 1070 Teeter, L., Hamme, R. C., Ianson, D., & Bianucci, L. (2018). Accurate Estimation of Net
1071 Community Production From O₂/Ar Measurements. *Global Biogeochemical Cycles*,
1072 32(8), 1163-1181.
- 1073 Teira, E., José Pazó, M., Serret, P., & Fernández, E. (2001). Dissolved organic carbon production
1074 by microbial populations in the Atlantic Ocean. *Limnology and Oceanography*, 46(6),
1075 1370-1377.
- 1076 Thunell, R., Benitez-Nelson, C., Varela, R., Astor, Y., & Muller-Karger, F. (2007). Particulate
1077 organic carbon fluxes along upwelling-dominated continental margins: Rates and
1078 mechanisms. *Global Biogeochemical Cycles*, 21(1).
- 1079 Tortell, P. D., Asher, E. C., Ducklow, H. W., Goldman, J. A. L., Dacey, J. W. H., Grzymski, J.
1080 J., et al. (2014). Metabolic balance of coastal Antarctic waters revealed by autonomous
1081 pCO₂ and Delta O₂/Ar measurements. *Geophysical Research Letters*, 41(19), 6803-6810.
- 1082 Uitz, J., Stramski, D., Reynolds, R. A., & Dubranna, J. (2015). Assessing phytoplankton
1083 community composition from hyperspectral measurements of phytoplankton absorption
1084 coefficient and remote-sensing reflectance in open-ocean environments. *Remote Sensing
of Environment*, 171, 58-74.
- 1086 Wang, S., Kranz, S. A., Kelly, T. B., Song, H., R., S. M., & N., C. (submitted). Lagrangian
1087 studies of net community production: The effect of diel and multi-day non-steady state
1088 factors and vertical fluxes on O₂/Ar in a dynamic upwelling region. *JGR-Oceans*.
- 1089 Yool, A., Martin, A. P., Fernandez, C., & Clark, D. R. (2007). The significance of nitrification
1090 for oceanic new production. *Nature*, 447(7147), 999-1002.
- 1091
- 1092
- 1093

1094 *Table 1: Production metrics for CCL-LTER Process cruises P1604 and P1706. Values represent average*
 1095 *rates in mmol C m⁻² d⁻¹ integrated over the mixed layer depth. Errors are standard errors of the mean*
 1096 *(SOM). ND indicates that no measurements were made. X indicates that data were not reliable as indicated*
 1097 *in the text.*

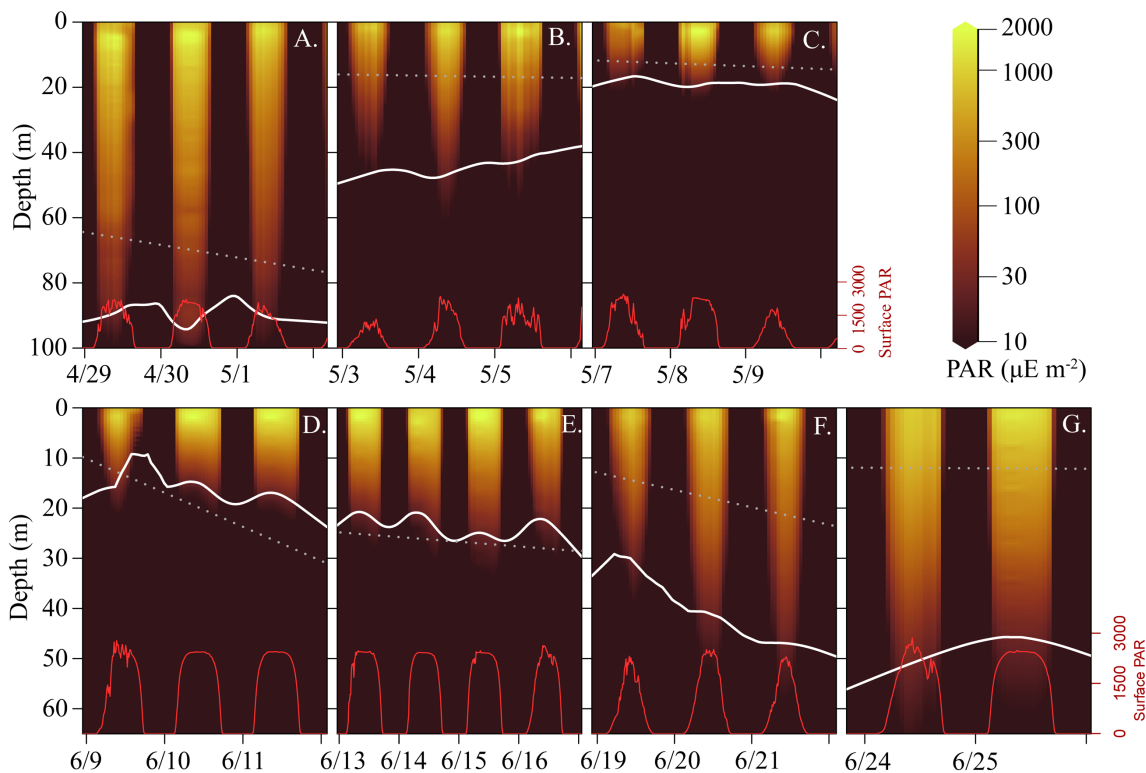
	NCP Prior	NCP inst	NPP _{14C}	NPP _{G/G}	NP	Export flux	f-ratio	GPP (FRRF)	GPP- EIMS	Respirati on (EIMS)
P1604										
Cycle 2	5.51 ± 0.25	6.02 ± - 0.13	17.7 ± 4.5	35.0 ± 5.8	10.6 ± 2.7	3.4	0.55 ± 0.06	ND	42.25 ± 9.3	57.25 ± 3
Cycle 3	-0.59 ± 5.61	-0.13 ± 1.18	48.4 ± 8.4	61.9 ± 7.8	23.9 ± 8.0	10.0	0.44 ± 0.07	ND	124 ± X	131 ± X
Cycle 4	39.47 ± 3.99	16.37 ± 4.04	126.4 ± 23.4	ND	22.9 ± 5.9	20.9	0.16 ± 0.01	ND	348 ± 158	418.35 ± 190.16
P1706										
Cycle 1	58.89 ± 1.24	77.84 ± 0.5	511.5 ± 150.1	524.1 ± 142.1	156.8 ± 19.2	29.3	0.34 ± 0.09	767.2 ± 148	1082 ± 134	1278.67 ± 76.93
Cycle 2	-12.23 ± 8.57	-14.26 ± 11.32	256.3 ± 27.9	269.2 ± 44.1	101.6 ± 44.0	44.5	0.40 ± 0.14	502.9 ± 92	401.1 ± 52.3	554.25 ± 101.32
Cycle 3	-11.8 ± 33.05	-10.47 ± 4.29	70.4 ± 21.9	76.7 ± 39.1	29.3 ± 18.5	46.7	0.49 ± 0.26	92.4 ± 12.8	X	X
Cycle 4	-0.19 ± 1.16	-0.07 ± 0.28	18.5 ± X	22.00 ± 6.4	5.4 ± 0.1	35.7	0.27 ± X	31.2 ± 1.4	X	X

1098

1101 **Figure 1.** Map of Lagrangian study sites for cruises P1604 (purple) and P1706 (red). P1604
1102 started in the west offshore and continues inshore, P1706 started in the east and continues further
1103 offshore. Colors indicate bathymetry.

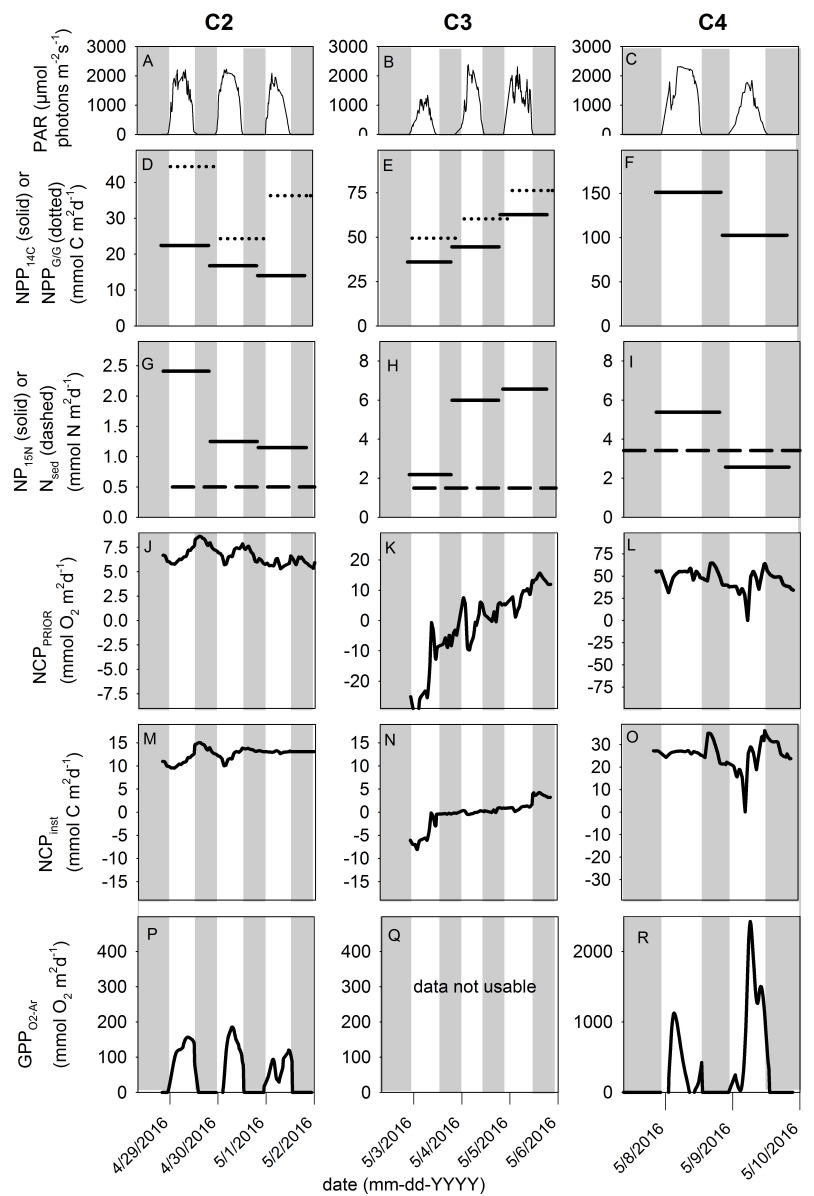


1104



1105

1106 **Figure 2.** Mixed layer depth and light levels for all experimental cycles (A. P1604-C2, B. P1604-C3, C.
 1107 P1604-C4, D. P1706-C1, E. P1706-C2, F. P1706-C3, G. P1706-C4). Red lines indicate surface PAR
 1108 intensity, colored shading indicate water-column light intensity ($\mu\text{mol photons m}^{-2}\text{s}^{-1}$), white solid line
 1109 indicates depth of the 1% light level, and dotted line indicates the mixed layer depth.



1110
1111 **Figure 3.** Chronology of primary production estimates during P1604. Panels [A-C] depict light intensity during P1604-C2, C3
1112 and C4, respectively. Panels [D-F] represent NPP derived from ^{14}C incubations (solid lines) and NPP_{G/G} from dilution
1113 incubations (dashed lines). Panels [G-I] show new production (from ^{15}N incubations; solid lines) and export production from
1114 sediment traps (dashed lines). Panels [J-L] show mixed layer NCP_{Prior}. Panels [M-O] show instantaneous air-sea biological O₂
1115 flux. Panels [P-R] represent calculated GPPs during the diel cycles as measured by NCP_{inst}. Note changes in scales and units as
1116 indicated by the axis labels. Data in panels D-I are integrated over 24 h and mixed layer depth. Data in panels A-C and J-R are
1117 integrated over 30-min intervals.
1118

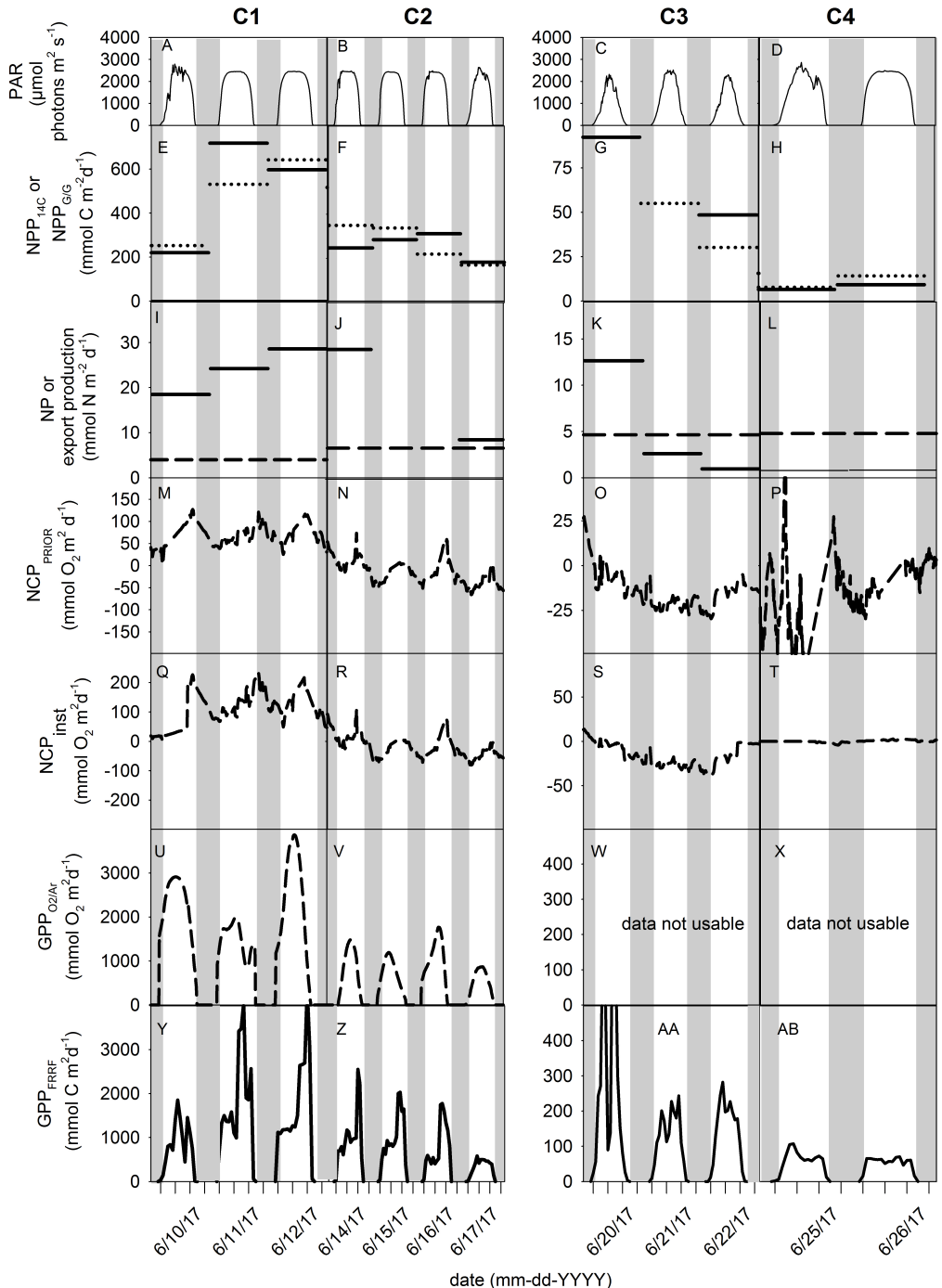
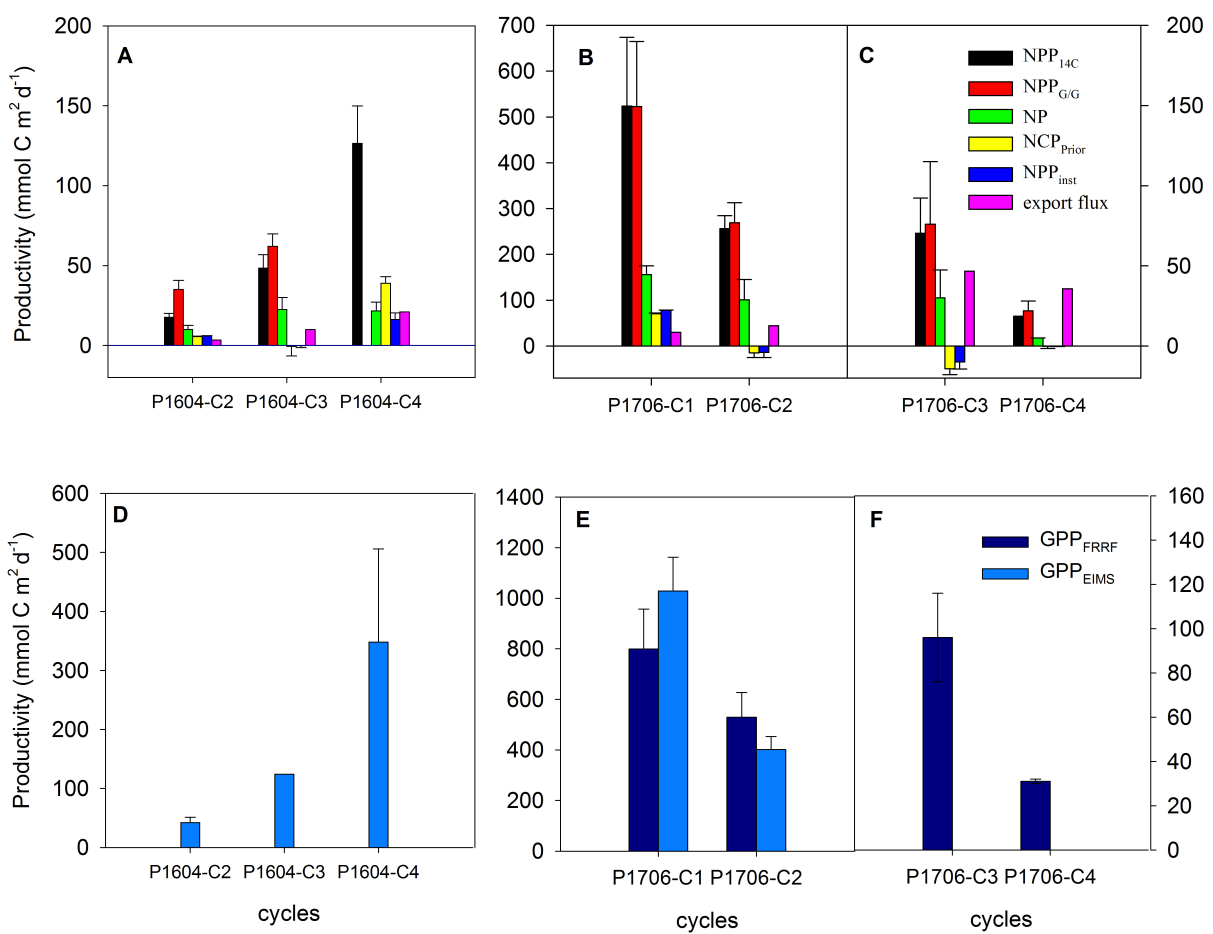


Figure 4.

1119
1120 Chronology of primary production estimates during P1706. Panels [A-D] depict the light intensity during the for
1121 cycles P1706-C1 to C4, respectively. Panel [E-H] represent NPP derived from ^{14}C incubations (solid lines) and the
1122 NPP_{G/G} from dilution incubations (dashed lines). Panels [I-L] show new production (from ^{15}N incubations) and export
1123 production from sediment traps. Panels [M-P] represent net community production measured with weighted k.
1124 Panels [Q-T] show net community production calculated using instantaneous k. Panels [U-X] represent calculated
1125 gross primary production from instantaneous NCP. Panels [Y-AB] represent gross primary production measured by
1126 FRRF. Note changes in scales and units as indicated by the axis labels. Data in panels E-P are integrated over 24 h
1127 and the mixed layer depth. Data in panels A-D and M-AB are integrated over 30-min intervals.



1128

1129 **Figure 5.** Summary of all production estimates. Data are normalized to carbon units. Note
 1130 difference in scales between the graph panels.